



A biophysical cortical column model to study the multi-component origin of the VSDI signal

S. Chemla^{a,b,*}, F. Chavane^b

^a NeuroMathComp Project, INRIA Sophia-Antipolis, 2004 route des Lucioles, 06902 Sophia-Antipolis, France

^b DyVA Team, Institut de Neurosciences Cognitives de la Mediterranee, CNRS, Aix-Marseille University, UMR6193, 31 Chemin Joseph Aiguier, 13402 Marseille, France

ARTICLE INFO

Article history:

Received 13 November 2009

Revised 28 May 2010

Accepted 9 June 2010

Available online 17 June 2010

Keywords:

Voltage-sensitive dye imaging (VSDI)

Biophysical model

Cortical column

Contrast response function (CRF)

NEURON simulations

ABSTRACT

We propose a biological cortical column model, at an intermediate mesoscopic scale, in order to better understand and interpret biological sources of voltage-sensitive dye imaging signal (VSD signal). To perform a quantitative analysis of the relative contributions to the VSD signal, a detailed compartmental model was developed at a scale corresponding to one pixel of optical imaging. The generated model was used to solve the VSD direct problem, i.e. generate a VSD signal, given the neural substrate parameters and activities. Here, we confirm and quantify the fact that the VSD signal is the result of an average from multiple components. Not surprisingly, the compartments that mostly contribute to the signal are the upper layer dendrites of excitatory neurons. However, our model suggests that inhibitory cells, spiking activity and deep layers contributions are also significant and, more unexpected, are dynamically modulated with time and response strength.

© 2010 Elsevier Inc. All rights reserved.

Introduction

Optical imaging comes within the scope of new imaging techniques that allow us to visualize the functioning brain at both high spatial and temporal resolutions. There are two main techniques (see Grinvald et al., 1999, for an introduction); the first is based on intrinsic signals which measure mostly absorption of the oxy- or deoxy-hemoglobin reflecting indirectly the neuronal activity, but also changes in scattering properties of the tissue. The second is based on voltage-sensitive dyes (VSDs), which bind to the membrane and transform variations in the membrane potential into optical fluorescence. The emitted fluorescence, recorded by a sensitive fast camera, is linearly correlated with changes in membrane potential per unit of membrane area of all the stained surfaces (Grinvald and Hildesheim, 2004), meaning all neuronal cells present in the cortex, but also all non-neuronal cells, such as glial cells. Neuronal cells include excitatory cells (e.g. pyramidal cells, spiny stellate cells) and inhibitory cells (e.g. basket cells, chandelier cells), whose morphology and intrinsic properties are quite different. Furthermore, each cell has various compartments, including dendrites, somata and axons. The measured signal is therefore a multiplexed signal that combines all these components. It is not straightforward to predict the result of the combination of such a large amount of intermingled components. Prediction of the origin of the VSD signal is also complicated by non-linearities in neuronal interaction. One important

example of these non-linearities is coming from inhibition that mostly acts in a divisive manner through shunting of the post-synaptic recipient, without clear hyperpolarization of the membrane potential (Borg-Graham et al., 1998). In other terms, a strong inhibition will not obligatory induce a net decrease of the VSDI signal. Therefore, although the underlying mechanism of the VSDI is well understood (Roland, 2002; Grinvald and Hildesheim, 2004), the recorded signal remains very complex and it is difficult to isolate the relative contributions of its different components (see Chemla and Chavane, 2010, for a specific review of the method limitation).

In this paper, our aim is to better understand the origin of the VSD signal (see Fig. 1A): what is the exact participation of the various neuronal components to this population signal? In particular, are excitatory and inhibitory cells participating equally for different levels of activity? What is the ratio between spiking and synaptic activity? Is this ratio the same when the network is at low vs. high levels of activity? What is the respective participation of cells from deep vs. superficial layers?

To answer those questions, our strategy has been to develop a biophysically inspired model to reproduce the optical imaging signal (see Fig. 1B). We modeled in detail one cortical column of 50 μm , which is one optical imaging averaged pixel size. This scale also corresponds to the spatial scale of the biological experiments (Markram et al., 1998; Gupta et al., 2000; Thomson et al., 2002; Thomson and Bannister, 2003), which were used to establish the precise local connectivity rules of columnar organization (Binzegger et al., 2004; Douglas and Martin, 2004; Hauesler and Maass, 2007) (red connectivity arrows, Fig. 1B). To embed this isolated column into a larger, hence more realistic, cortical network, we simulated an additional synaptic bombardment according

* Corresponding author. Present address: Canadian Centre for Behavioural Neuroscience, The University of Lethbridge, 4401 University Dr W, Lethbridge, AB, Canada, T1K 3M4.

E-mail address: sandrine.chemla@uleth.ca (S. Chemla).

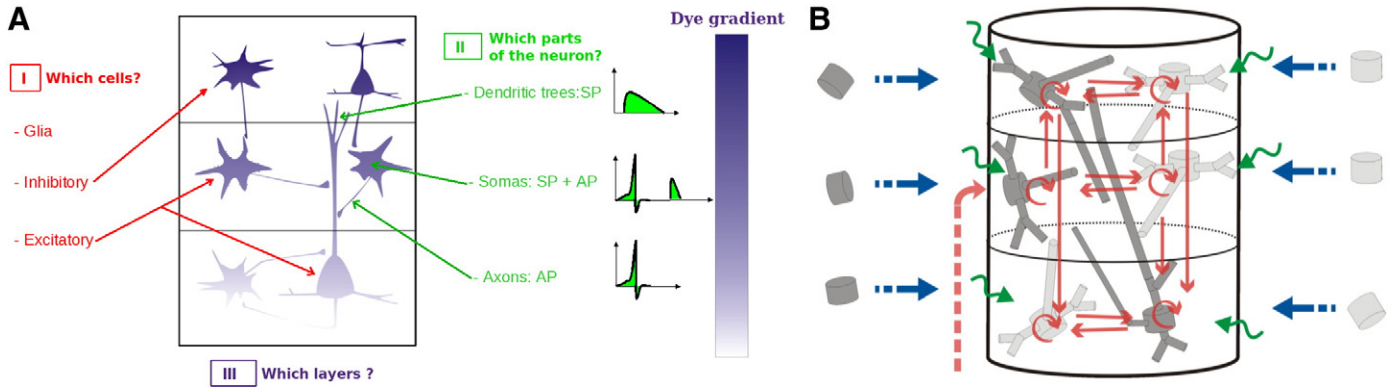


Fig. 1. Rationale and detail of the model. **A:** Contributions to the optical signal. Once neurons are stained by the VSD, every neuronal membrane contributes to the resulting fluorescent signal, but from where? and in which proportions? Answering these four questions could clarify the optical signal origins: 1) Which cells? 2) Which parts of the cell? 3) Which layers? 4) Which presynaptic origins? **B:** Schematic view of the cortical column model. Six specific populations of neurons: excitatory (dark gray) and inhibitory (light gray) populations in each of the three layers (2/3, 4, and 5/6). Thalamic afference to layer 4 cells is symbolized by a dashed red arrow, while local connectivity within the model is inspired from Binzegger et al. (2004) and has been sketched by red arrows (for clarity, only the main connections are represented). To obtain a more realistic behavior of our column, we added fluctuating conductances that mimic synaptic bombardment according to Destexhe et al. (2001), here cartooned as green arrows. Finally, the isolated column has been embedded in a larger network by simulating horizontal afferences from a large V1 network by random spike trains whose latency, frequency, and synaptic weight are tuned to fit data from Buzas et al. (2006), depicted here as blue arrows.

to Destexhe et al. (2001) (green arrows, Fig. 1B). Four types of neurons were considered with only two distinct firing patterns, regular spiking and fast spiking, since they are known to be respectively the great majority of excitatory (dark gray, Fig. 1B) and inhibitory cells (light gray, Fig. 1B) in the neocortex (Contreras and Palmer, 2003). To tease apart the different contributions of the various components of the signal, we dynamically explored functional parameters that are known to affect differentially those components. Among all parameters, we decided to manipulate the activity level (here thalamic input rate, dashed red arrow, equivalent to contrast) both at the single neuron and the global network level. These manipulations were applied within functional regimes that are known to affect differentially excitatory (RS cells) and inhibitory (FS cells) components of the network, but also the relative contribution of membrane depolarization and spiking output.

In this article, we first describe the proposed model of cortical column chosen to analyze biological sources of the optical signal, then we discuss its behavior and its application for VSD signal computation. We finally answer the previous questions.

Material and methods

Single neuron model

Each neuron is represented by a reduced compartmental description (see Bush and Sejnowski, 1993, for more details on the reduction method) with conductance-based Hodgkin–Huxley neuron model (Hodgkin and Huxley, 1952) in the soma and the axon. The dynamics of single cells are described by the following equation:

$$C_m \frac{dV}{dt} = I_{ext} - \sum_i G_i(V)(V - V_i) \quad (1)$$

where V is the membrane potential, I_{ext} is an external current injected into the neuron, C_m is the membrane capacitance, and where three types of current are represented: leak, potassium and sodium conductances or respectively G_L , G_K and G_{Na} . G_L is independent of V and determines the passive properties of the cells near resting potential. The sodium and potassium conductances are responsible for the spike generation.

A slow potassium conductance (called M-conductance) was also included in the dynamics of the excitatory population to reproduce the observed adaptation of the spike trains emitted by these neurons (Nowak et al., 2003). This feature seems to be absent in inhibitory neurons (Contreras and Palmer, 2003), as taken into account in this work.

Only passive dendrites were considered. Each neuron is represented with eight to ten compartments. The link between two adjacent compartments j and k can be described by Eq. (2) (Hines and Carnevale, 1997).

$$C_j \frac{dV_j}{dt} + I_{ion_j} = \sum_k \frac{V_k - V_j}{R_{jk}} \quad (2)$$

where V_j is the membrane potential in compartment j , I_{ion_j} is the net transmembrane ionic current in compartment j , C_j is the membrane capacitance of compartment j and R_{jk} is the axial resistance between the centers of compartment j and adjacent compartment k .

Network architecture and synaptic interactions

We consider a class of models based on a cortical microcircuit (see Raizada and Grossberg, 2003; Douglas and Martin, 2004; Haeusler and Maass, 2007, for more details on this concept), whose simplified synaptic connections are made only between six specific populations of neurons: two populations (excitatory and inhibitory) for three main layers (II/III, IV, and V/VI). Thanks to the NEURON software¹ and its Model DB database, providing an accessible location for storing and efficiently retrieving computational neuroscience models, we have been able to reconstruct four types of neurons (Bush et al., 1999): small pyramidal cells in layer II, spiny stellate cells in layer IV, large pyramidal cells in layer V and smooth stellate cells in all layers. More precisely, the chosen model is a model of 180 neurons, 143 excitatory neurons: 50 small pyramidal (SP) in layer II/III, 45 spiny stellate (SS) in layer IV, 48 large pyramidal (LP) in layer V/VI, and 37 inhibitory neurons of one unique type: respectively 14, 13, 10 smooth stellate in layers II/III, IV, V/VI (SmS2, SmS4, and SmS5). The difference in morphology and membrane surface of these different neuronal types was then taken into account when computing the VSD signal (see computation of the VSD signal).

Synaptic inputs were modeled as conductance changes. Excitatory AMPA synapses are converging on dendrites of each neuron, whereas inhibitory GABA_A synapses are converging on soma of each neuron (see Salin and Bullier, 1995 for a review on the subject). The number of synapses involved in the projections between these different neuronal types, including the afferent from the LGN (X/Y) (recalculated for 50 μ m cortical column), were based on Binzegger et al. (2004, see Fig. 12) for the considered layers while latencies have been introduced for each connection, following Thomson and Lamy (2007). This network

¹ <http://neuron.duke.edu>.

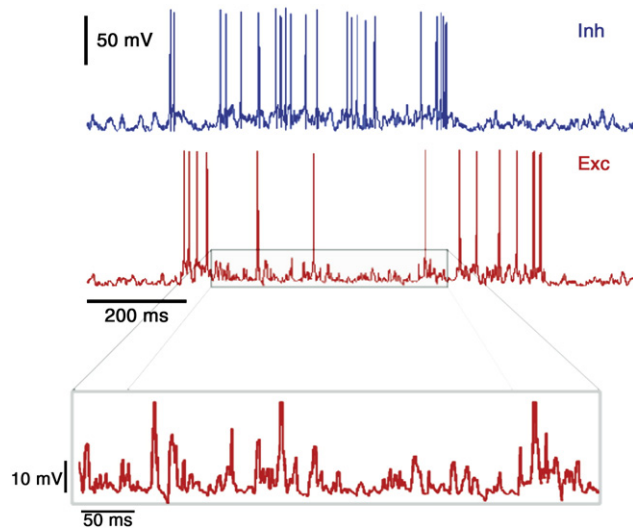


Fig. 2. Inhibition operates in a shunting mode. Within the full network, the presynaptic inhibitory neuron (upper trace) shunts the activity of the post-synaptic excitatory neuron (lower trace). When zooming (lower panel), we verify the “silent” effect of this inhibition since no net hyperpolarization is visible.

architecture was built using the neuroConstruct software² and run on the NEURON simulator. A schematic view of the model is given in Fig. 1B. Note that, as synaptic inputs are conductance-based and that the GABA_A reversal potential was chosen equal to the resting potential (−70 mV), our inhibitory interactions are mostly shunting and not hyperpolarizing (see Fig. 2). It has been indeed documented that inhibitory interactions are acting in a silent, shunting mode (Borg-Graham et al., 1998; Anderson et al., 2000; Fregnac et al., 2003). As VSDI signal reports changes of membrane potential, it was important to verify that the inhibition implemented in the model acts silently without net hyperpolarization.

Thalamic afferents, background activity and lateral interactions

Input signals from the thalamus into the neocortex layer IV are simulated by applying 10 random spike trains (Alonso et al., 2001) to each neuron in layer IV (45 SS + 13 SmS4 neurons) (dashed red arrow, Fig. 1B). Latencies were chosen randomly within a given temporal window (initially tested from 0 to 10 ms with a uniform distribution, and changed from 0 to 50 ms, see Results section) for each input connection, to reproduce the temporal properties of the geniculocortical pathway according to Reid and Alonso (1996). Rate of the thalamic input was manipulated to study the influence of cortical regime on the relative contributions of the different compartments (see details in Results section). At a first approximation, this simplest assumption on the thalamic drive describes well the thalamic discharge statistics (Gazeres et al., 1998). We also introduced synaptic depression in our thalamo-cortical synapses in order to scale down the input activity range (0–100 Hz). We used the NEURON implementation of a model of short-term synaptic plasticity based on the kinetics described by Tsodyks et al. (1998). Note that the mechanism implemented here uses a conductance change instead of current sources to represent synapses. At this point, the column is isolated.

In order to embed this column into a larger network, we proceeded as follows. First, “background noise” was introduced in each neuron of the column (green arrows, Fig. 1B). Typically, noise can be introduced in the form of stochastic fluctuation of a current or an ionic conductance. The stochastic model of Destexhe et al. (2001), containing two fluctuating conductances, is used here, allowing us

to simulate synaptic background activity similar to in vivo measurements for a large network. The mean spontaneous firing rate and the mean resting membrane potential of the neurons were adjusted according to Monier et al. (2003) database.

Second, as the introduction of background activity was not sufficient to account for the observed experimental signal time course (see Results), an entire hypercolumn of about 750 μm was simulated by introducing lateral interactions between neighboring columns. This was done by introducing a convergent horizontal input to our column which was de-correlated to the column neuronal activity (blue arrows, Fig. 1B). This input consisted in another set of random spike trains that are delayed in time to fit the known velocity of horizontal axons and tuned in strength and synapses numbers to fit the literature (Buzas et al., 2006, see Results).

Single neuron analysis

The spiking contribution for each input frequency was calculated as follows: first, spikes were detected on intracellular recording with a threshold of 0 mV. For each neuron, post stimulus time histograms (PSTH) were then computed over all trials with 10 ms bin precision during 1000 ms including 600 ms of evoked activity. We also averaged the PSTH over a given subpopulation of neurons (for example, excitatory and inhibitory classes in Figs. 4A,B,C, or different layers in Figs. 5C and 9).

To compare these subpopulations spiking activity to the global VSD signal, correlation coefficients were computed at the trial-by-trial level (Fig. 9). Here, spiking activity was pooled from all neurons belonging to one subpopulation for a given trial to compute a global PSTH at a 10 ms bin precision. Then, this trial-based population PSTH was compared to the modeled VSD signal binned at the same temporal precision (10 ms). A correlation coefficient was computed between these two time series for three different time windows ([−200 −20]; [0 50]; [50;500]) and averaged on 30 trials.

The membrane potential contribution for each input frequency was calculated as follows: the membrane potential of each neuron was recorded at the middle of each of its compartments. To compute the contributions of a given component (excitation, inhibition, soma, layers, etc.), we then averaged the membrane potential over all the considered compartments. For example we averaged the membrane potential over all dendritic compartments of layer II neurons to compute the overall subthreshold dendritic contribution of neurons in superficial layer II.

Similarly to the spiking contribution, the subthreshold activity of each compartment was also compared to the global VSD signal using a trial-by-trial correlation analysis (Fig. 8). Correlation coefficients were computed between the two time series at the same temporal precision (0.1 ms), for three different time windows ([−200 −20]; [0 50]; [50;500]) and averaged on 30 trials.

Computation of the VSD signal

The VSD signal was simulated using a linear integration over the membrane surface of all neuronal components (Grinvald and Hildesheim, 2004). Here, the use of compartmental model has a real interest since the computation of the VSD signal, for a given layer L , is given by:

$$OI^L = \lambda^L \sum_{i=0}^{N^L} V_i(0.5)S_i \quad (3)$$

where N^L is the number of compartments in layer L , S_i is the surface of the i th compartment, $V_i(0.5)$ is the membrane potential taken in the middle of the i th compartment, and λ^L represents the fluorescence's gradient or the illumination intensity of the dye in layer L . We reported in Table 1 the values of total membrane surface of each of the modeled neurons. For information, we also reported what we called

² <http://www.neuroConstruct.org>.

Table 1

Membrane surface and fluorescence emission capacity (membrane surface scaled by staining gradient) of the modeled neuronal types.

Neurons	Pyramidal L2	Pyramidal L5			Spiny stellate L4	Smooth stellate		
		L2	L4	L5		L2	L4	L5
Number	50	0	0	48	45	37	37	37
Total membrane surface (μm^2)	8218.4	1570.8	9180.3	21971.5	6694.7	6694.7	6694.7	6694.7
Fluorescence emission capacity (arbitrary units)	7807.4	1492.2	459	0	334.7	6359.9	334.7	0

“fluorescence emission capacity” which is simply the membrane surfaces scaled each by the staining gradient (i.e. $S_{tot}\lambda^L$). A detailed illustration of the construction of VSD signal from our compartment's activity is shown in [Supplementary Fig. 1](#).

We thus can take into account soma, axon and dendrites influences, introduce 2D geometrical properties (dendrites of large pyramidal neurons in layer V can reach superficial layers) and fluorescence's gradient depending on depth. According to [Lippert et al. \(2007\)](#) and [Petersen et al. \(2003\)](#), we chose to take $\lambda^2 = 0.95$, $\lambda^4 = 0.05$ and $\lambda^5 = 0$. Note that in [Lippert et al. \(2007\)](#), this corresponds to dye diffusion in the rat without dura removal which might differ from data in higher mammal species (see [Discussion](#) section). Then, the total optical imaging signal is given by the following formula:

$$OI = \sum_{L \in \{\text{Layers}\}} OI^L \quad (4)$$

For our model, we computed the fractional signal ($\Delta F/F$) as done experimentally [Reynaud et al. \(2007\)](#): we first transformed the level of depolarization into amount of fluorescence (i.e. number of photons) using an arbitrary linear transformation ($F = aV + b$ with $a = 1$ and $b = 100$) which is a first realistic approximation. Indeed, it is the simplest choice to make sure that all compartments contribute positively to the global signal, while it assumes that one photon is emitted for each 1 mV increase of membrane potential. Then we simulated the VSD signal in term of relative fluorescence by taking relative variations of fluorescence (ΔF) compared to the resting level (F) observed at rest. Note that this fractional signal is in arbitrary units as it all depends on the parameter set (a and b) used to transform voltage in fluorescence.

Results

Model behavior and quantitative adjustments

As mentioned in the [Introduction](#), our idea is to evaluate the contribution of the various components of the VSD signal as a function of activity level. It was therefore mandatory to develop a model that behaves realistically in response to different levels of activity, both at the single neuron and the global network level. We thus started by fitting the model to intracellular recordings references providing information about subthreshold but also spiking activity as a function of the level of input activity.

Single neuron regimes

We adjusted the intrinsic properties of our isolated neurons to fit those shown in [Nowak et al. \(2003\)](#) from *in vivo* intracellular recordings. For each neuron, the optimized parameters were the channel conductances G_i , and the passive electrical properties of compartments: the specific axial resistance R_a and the specific capacitance C_m . The optimization algorithm used was the PRAXIS (principal axis) method described by [Brent \(1976\)](#) and embedded into the NEURON software. The parameter values are given in the table of [Fig. 3C](#). Excitatory and inhibitory neurons were modeled to have regular spiking (RS) and fast spiking (FS) intrinsic properties, since RS and FS cells are known to be respectively the great majority of

excitatory and inhibitory cells in the neocortex ([Contreras and Palmer, 2003](#)). [Fig. 3](#) shows the action potential shapes of RS cells and FS cells of the model, showing that RS cells fired action potentials of 1 ms duration ([Fig. 3A, left](#)) measured at threshold, whereas FS cells ([Fig. 3A, right](#)) had short-duration action potential (0.5 ms at threshold), as documented in the literature ([Contreras and Palmer, 2003](#)). Examples of action potential responses to depolarizing current injection in these two populations are also plotted. Here, RS cells ([Fig. 3B, left](#)) produced adapting spike trains at about 60 Hz, whereas FS cells ([Fig. 3B, right](#)) generated high frequency train of spikes at about 300 Hz with pronounced and brief spike after hyperpolarizations (AHPs) that fits properly the electrophysiological data from [Nowak et al. \(2003\)](#) and [Contreras and Palmer \(2003\)](#).

From these action potential responses, we calculate the relationship between injected current intensity (in nA) and the total firing rate (in spikes per second). The slope (in Hz/nA) of the linear regression characterizes the current–frequency relationship of the neuron ([Fig. 3D](#)), which is one of the useful characteristics in distinguishing between different types of neurons, as explained by [Nowak et al. \(2003\)](#), especially RS and FS cells. This slope is considerably steeper in the FS cell (375 Hz/nA) compared with that for the RS cell (83.3 Hz/nA), in accordance with what is shown in [Nowak et al. \(2003\)](#) (519 Hz/nA for the FS cell and 85 Hz/nA for the RS cell).

Local network calibration

The next step in the validation of the model is at the level of the whole connected local network of neurons. To calibrate this network at different working regimes, we chose to compare the input–output relationship predicted by the model to the contrast response function (CRF) of V1 neurons classically recorded electrophysiologically, as done in [Contreras and Palmer \(2003\)](#). The CRF describes the fact that cortical cells adjust non-linearly their response to an input with increasing strength ([Albrecht and Hamilton, 1982](#)). Non-linearities in the CRF (compression and saturation) allow cortical cells to adjust the useful dynamic response to an operating range of contrasts that can be modulated. This control is supposed to be adjusted by a dynamic balance between excitation and inhibition. Our manipulation of input strength was simply to increase the thalamic rate. The correspondence between input strength in contrast vs. spiking input rate is not straightforward. Therefore, we chose to adjust our model at saturation level for which the network regimes can be compared, and only made qualitative comparison for the rest of the response curve. The related parameters to be adjusted are then the weight values of synaptic connections, w_{EE} , w_{EI} , w_{IE} and w_{II} for connections between excitatory neurons, from excitatory neurons onto inhibitory neurons, from inhibitory onto excitatory neurons and between inhibitory neurons respectively. This is done using the PRAXIS optimization algorithm again. We obtain an interval for each of the four weight values by fitting both the spike rate and the membrane potential of the two populations, in response to contrast input, i.e. input rate. Then we generate uniformly distributed random numbers over this specific interval.

Input–output functions of excitatory and inhibitory population of neurons, predicted by the model and obtained both with spike rate and membrane potential are reported in [Figs. 4A,D](#). We observe that

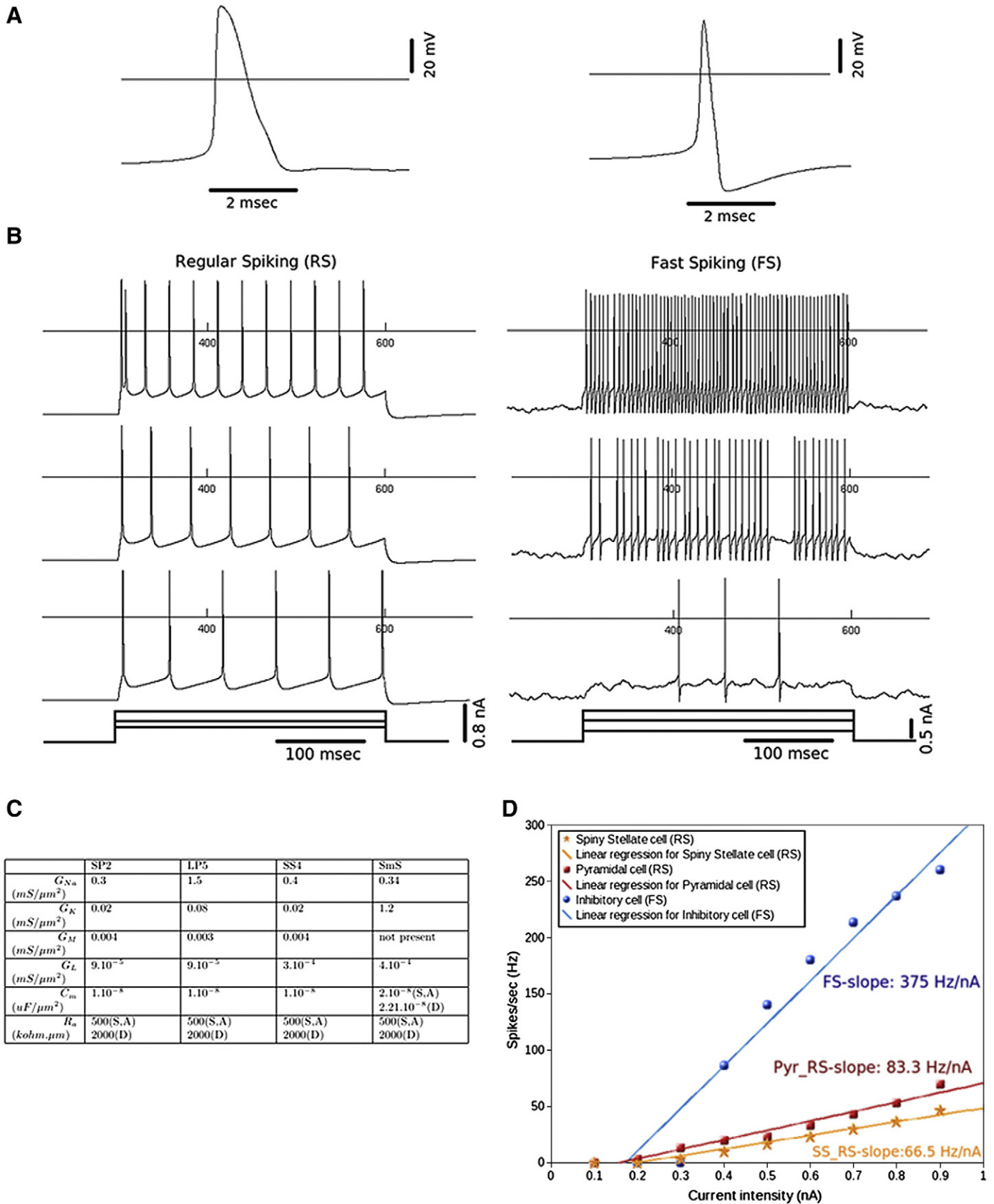


Fig. 3. Adjustment of electrophysiology properties of isolated neurons. **A:** action potential shape of regular and fast spiking cells. Left: regular spiking (RS) cell. Right: fast spiking (FS) cell. **B:** examples of action potential responses to depolarizing current injection in the two main classes of cortical neuron of our model, fitted with intracellular recording from Nowak et al. (2003). Left: regular spiking (RS) cell. Right: fast spiking (FS) cell. **C:** values of neurons parameters for the four types of neurons: small pyramidal cell in layer II (SP2), large pyramidal cell in layer V (LP5), spiny stellate in layer IV (SS4) and smooth stellate inhibitory cell (SmS). G_{Na} , G_K , G_{sl} and G_L are respectively sodium, potassium, slow potassium and leak conductances. C_m is the specific membrane capacitance and R_a is the specific axial resistance (S, A, and D for respectively Somas, Axons and Dendrites compartments). **D:** firing rate vs. current intensity (f-I curves) for the cells shown in Fig. 1B. Each point is the average of the mean firing rate for 5 repetitions of a given current intensity.

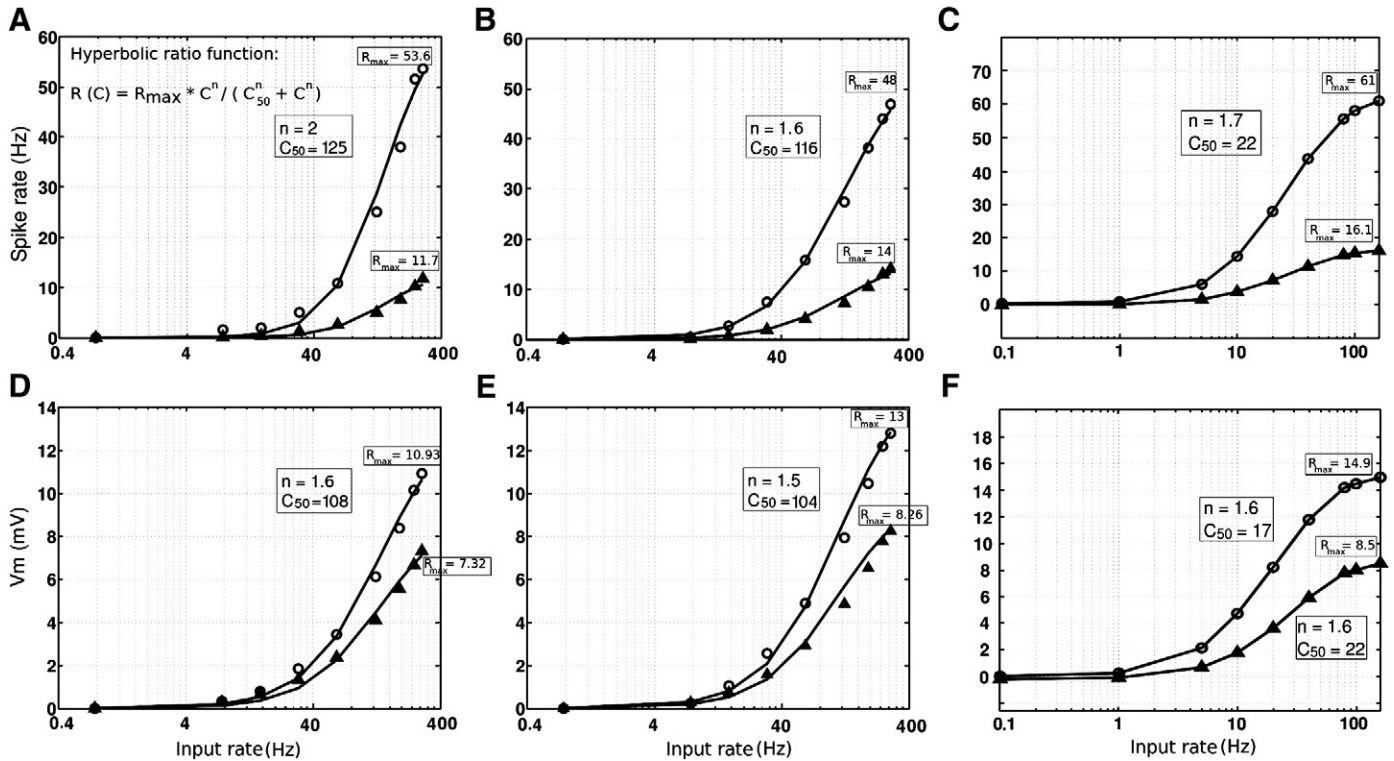


Fig. 4. Input–output function of excitatory (RS cells: filled triangles) and inhibitory (FS cells: open circles) population of neurons, obtained with spike rate and membrane potential, in a isolated column (A,C), after lateral interactions introduction (B,D), and after introduction of synaptic depression at the thalamo-cortical synapses (E–F). Each point is the average of the mean quantity for 10 repetitions of a given input rate. A,B,C: spike rate. D,E,F: membrane potential (Vm). Each input–output spiking rate function is fitted by an hyperbolic ratio function (black curves). The values of the parameters n , C_{50} and R_{max} are reported on the figure for each case.

these curves are very similar to the CRFs obtained electrophysiologically in Contreras and Palmer (2003) for the two main populations of neurons (RS and FS cells). As the authors suggested, the input–output functions are best fitted by an hyperbolic ratio function (see black lines in Fig. 4), also known as the Naka–Rushton equation of the form:

$$R(C) = R_{max} \cdot \frac{C^n}{C_{50}^n + C^n} \quad (5)$$

where R denotes the response of the cell and C the contrast levels. We use the values of the exponent n , the semi-saturation contrast C_{50} and the maximum value of the response R_{max} , i.e. parameters of the hyperbolic ratio function, to quantify the quality of the fit. These three values are reported on each plot. As concluded by Contreras and Palmer (2003), there are no significant differences between the values of n and C_{50} obtained from spike responses and those obtained from membrane potential responses. However, at this stage, we were surprised to reach so high semi-saturation input rates (more than 100 Hz). Indeed, we tuned our model such as (i) inhibition was clearly but realistically dominating excitation at high level activity regimes (Fig. 3D) and (ii) acting in a divisive, shunting, manner (Fig. 2). These parameters were not enough though to clearly saturate cortical response at high input rate. As suggested by Carandini et al. (2002), we then decided to introduce a synaptic depression term at the thalamo-cortical synapses (see Material and methods). Synaptic depression introduction at the neuronal level efficiently scaled down the input activity range (0–100 Hz), as shown in Fig. 4C. Moreover, both responses (spike rate and Vm) now exhibited a clear saturation at high frequency, as observed in electrophysiological contrast response functions (Contreras and Palmer, 2003). Semi-saturation input rates were scaled down to more realistic ranges, with no significative difference between spiking and membrane potential responses, or FS and RS cells (22 and 17 Hz).

To differentiate the two cells groups, the only important differences are in R_{max} obtained with spike rates, higher in FS cells (53.6 Hz) than in RS cells (11.7 Hz), as also obtained by the authors (59.4 Hz vs. 8 Hz respectively). Exponent n values are also similar between our model and real neurons (1.6 vs. 2.03 for membrane potential and 2 vs. 2.15 for spike rate). Note that values of R_{max} and n were not affected by the incorporation of the synaptic depression parameter.

The resulting biophysical model is thus a balanced local network of detailed neurons (80% of RS cells and 20% of FS cells in the three main layers of the cortex), with thalamic inputs and background activity. We can now proceed and compute the VSD signal from the depolarization of all our compartments of the well tuned model. In Fig. 5 we show the gradual build-up of the VSD signal, from thalamic afference (A), activating post-synaptic cortical cells (B and C), resulting in a global VSD increase of fluorescence (D) with a delay in general between 5 and 10 ms.

We will now first verify the adequacy of the model by comparing our model dynamics with the same curves obtained experimentally. Thereafter, two different quantitative explorations of the origins of the VSD signal will be explored thanks to the neuronal compartmentalization of our model. A first correlation analysis will be devoted to dissect the neuronal elements that mostly influence the global signal dynamics. A second application will be to quantitatively predict the relative contributions of the various VSD signal sources for increasing level of thalamic input.

Temporal evolution of the modeled VSD signal

We simulated the VSD signal in response to focal stimuli, and compared it to experimental results obtained by Reynaud et al. (2007). In this experiment, the visual stimuli, a small luminance Gaussian (0.5 standard deviation) is presented to a behaving monkey during 800 ms whose task was simply to fixate a dot for the whole

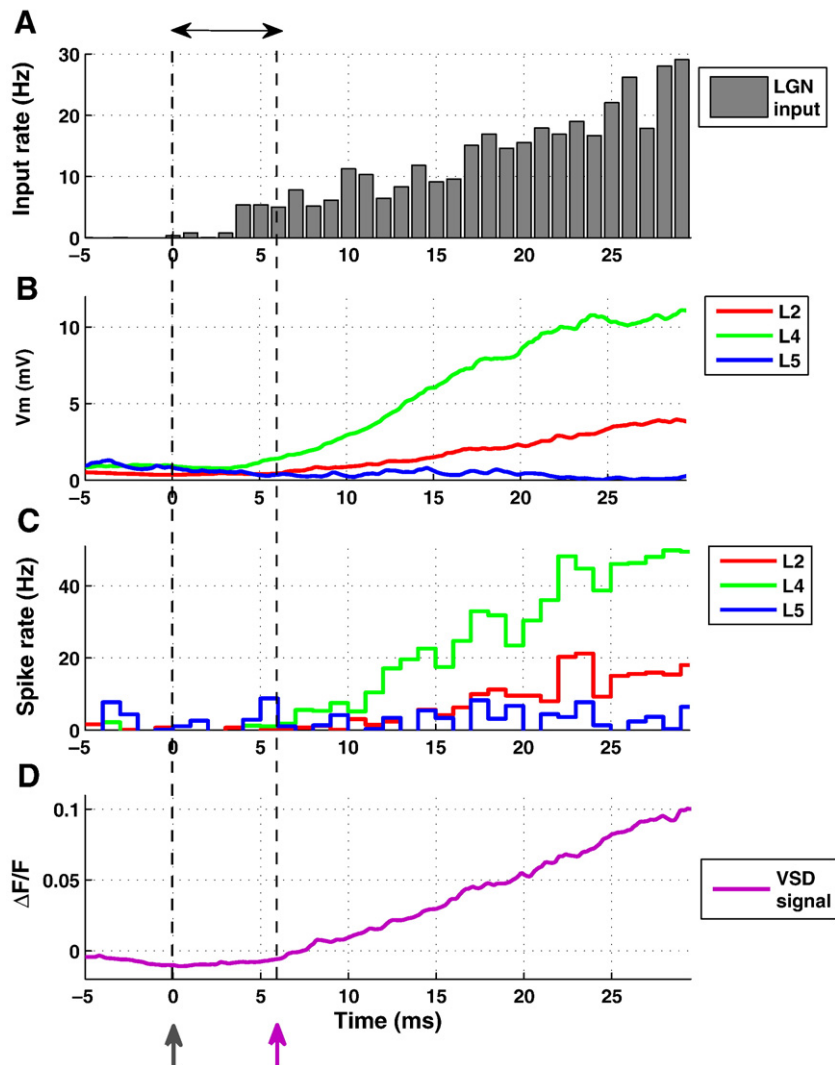


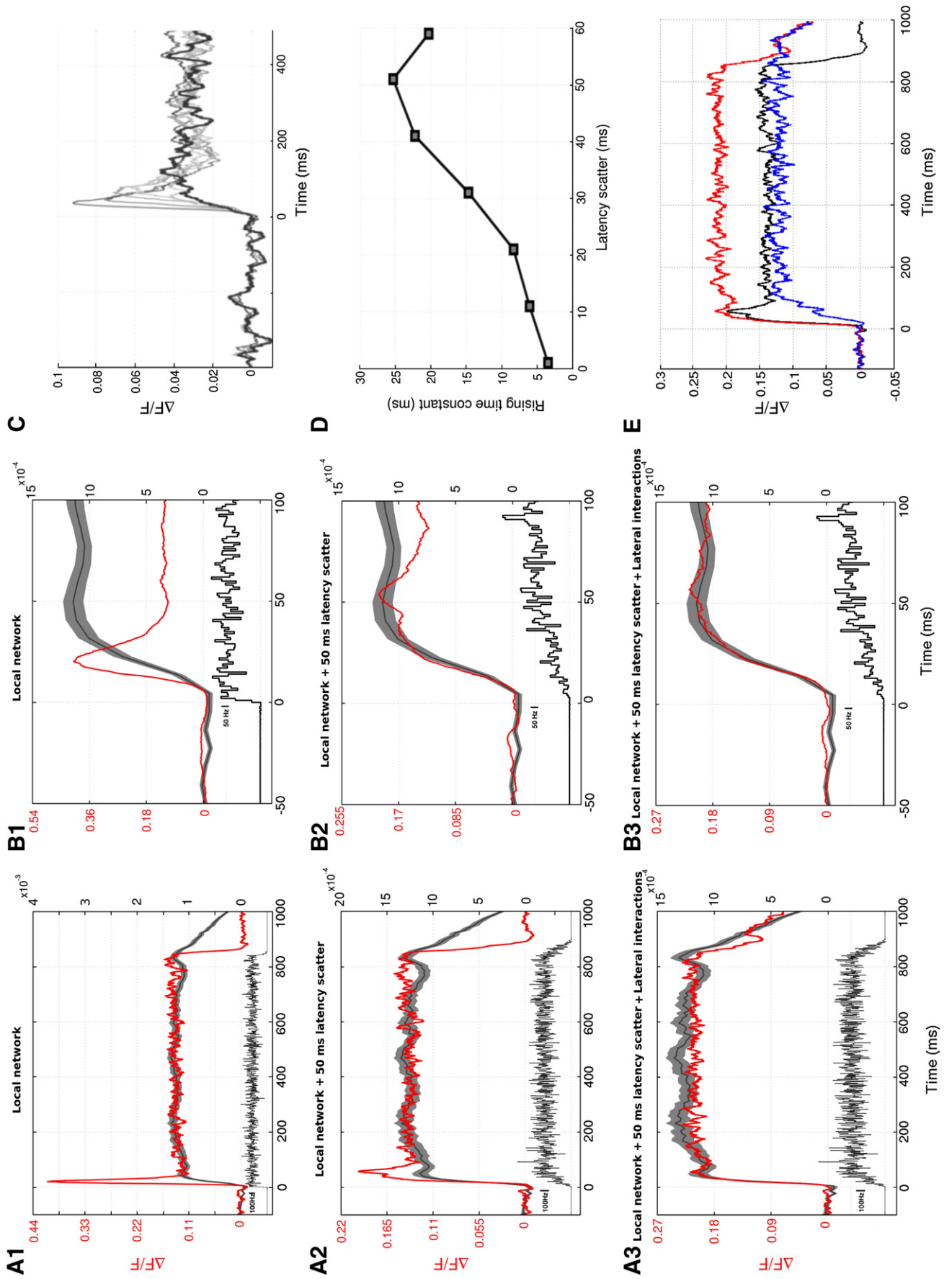
Fig. 5. From thalamic input to the VSD signal. A: Post Stimulus Time Histogram of the thalamic afference to our model for the early part of the evoked response. Time 0 is the start of the stimulation. B: the thalamic afferent are integrated by post-synaptic cells in our column inducing a depolarization after a certain delay in layer IV neurons (green) followed by layer II neurons (red) and layer V neurons (blue). C: this post-synaptic depolarization induces spiking activity that we depict with a hollowed-up PSTH with similar colorcodes. D: these activities lead to a global VSD response that starts with typical delays of 5–10 ms after thalamic onset.

duration of the experiment. Fig. 6A shows the temporal evolution of the modeled VSD signal (red line) in response to the thalamic afference (post stimulus time histogram (PSTH) at the bottom) which is compared to the experimental results obtained on monkey using VSDI (the mean curve is plotted in black while standard errors are represented by the gray area).

The time course of the modeled signal in response to an abrupt change of the input is faster than the experimental one: the onset of the response shows a large transient *peak* followed by a *plateau* and

the transient offset is very sharp compared to the experimental one. Notice that in column A, the modeled signal is normalized to the sustained activity of the experimental signal, while in column B, it is normalized to its transient onset. What can be at the origin of such different dynamics? We first speculated that that the peak was due to a network synchronization at the response onset. We thus tested many parameters (membrane time constants of neurons, spontaneous activity, and connections weights), but only the input latency scatter introduced was efficient at desynchronizing the network and

Fig. 6. Temporal evolution of the VSD signal (red lines), from local to global network. Each curve is the average of the response for 50 repetitions. Mean responses obtained experimentally are superimposed to the modeled signal (dark gray lines with standard error in light gray), normalized to either fit the tonic (A1–A3) or the phasic (B1–B3) part of the signal. Experimental trace was obtained on averaging VSD signal over a small region of interest of V1 of an awake monkey, trained to fixate a central dot while a Gaussian of luminance was presented for 800 ms (0.5 standard deviation, maximal luminance 86 cd/m², background luminance of 14 cd/m²). Monkey was rewarded if correctly achieved fixation within a 1 × 1 tolerance window during the whole duration of the experiment. Thalamic afference (PSTH) is shown at the bottom of each figure (black trace). A1: the temporal evolution of the modeled VSD signal in response to an input of 800 ms is plotted as a function of time for a given input frequency (300 Hz). A2: the temporal evolution of the modeled VSD signal is replotted after the introduction of 50 ms latency scatter on LGN inputs. A3: the temporal evolution of the modeled VSD signal is finally replotted after lateral interactions introduction. B: zoom on the rising time course of the VSD responses: for the local network (B1), for the local network after introducing 50 ms latency scatter on LGN inputs (B2), and for the global network, i.e. after introducing the lateral connections (B3). C: influence of the latency scatter (from 0 to 60 ms with a step of 10 ms) of LGN inputs on the VSD responses (input frequency of 64 Hz). D: rising time constant plotted as a function of latency scatter. E: superimposition of local plus latency scatter (black), lateral (blue) and global VSD responses (red), providing quantitative contributions of local and lateral inputs to the total VSD signal.



slowing the rising time constant of the VSD signal. The analysis of this parameter to improve the rising time constant of VSD responses is described in Figs. 6C,D. The beginning of temporal responses is plotted for several values of the latency scatter (Fig. 6C, from 0 to 60 ms with a step of 10 ms). Then, in order to quantify the rising time constant of each response, we use an exponential fitting:

$$F(t) = a + k\left(1 - \frac{e^{-(t-\text{offset})}}{\tau}\right) + k2\left(1 - \frac{e^{-(t-\text{offset})}}{\tau2}\right) (t \geq \text{offset}) \quad (6)$$

where a , k , $k2$, τ , $\tau2$ and offset are the fit parameters. By plotting the rising time constant, i.e. the mean of τ and $\tau2$, as a function of the latency scatter (Fig. 6D), we obtain an optimal value of 50 ms, instead of the 10 ms first introduced (see the Material and methods section). This value is actually in accordance with several studies investigating the temporal latencies of non-lagged thalamic cells in response to retinal cells stimulation (Mastrorade, 1987; Hartveit and Heggelund, 1992; Saul and Humphrey, 1990), see recent review of Saul (2008). Increasing the latency scatter of the LGN inputs (see bottom PSTH) provides the expected effect, i.e. reducing the peak of the response onset (Fig. 6A2) and increasing the rising time constant (Fig. 6B2). The rising time constant of the modeled response (32.3 ms) is now much closer to the experimental one (35 ms). We have also noticed that the latency depends on the input frequency of the stimulus (we will nevertheless keep a constant value of 50 ms for all the input frequencies). However, the transient onset and offset of the VSD signal are still faster than the experimental one (notice the response offset in A2 and the zoom of the response onset in B2). Furthermore, the model response still contains a prominent phasic component not present in experimental data.

Our next hypothesis was that the discrepancy in time constants could come from the fact that we modeled an isolated column representing only one pixel of VSDI, compared to the experimental conditions where a whole cortical network integrates the visual stimulation, representing interactions across many pixels. Therefore, in order to take into account an entire hypercolumn of about 750 μm , we reproduced lateral connections existing between our column and its neighbor columns. Each neuron of our column receives excitatory and inhibitory inputs. These lateral inputs were simulated by using random spike trains whose frequencies were adjusted to the output frequencies of the local network. For example, one pyramidal cell in layer II receives spike trains from neighbors pyramidal and inhibitory cells also in layer II, and the frequency of these spike trains is given by the output mean frequency of pyramidal and inhibitory cells of our local column, for a given thalamic input. Synaptic weight of each lateral connection was adjusted proportionately to the cortical distance between neurons, also influencing the synaptic latency of the connection (Bringuier et al., 1999). Weight distributions for excitatory and inhibitory lateral connections were adjusted according to quantitative biological data taken from Buzas et al. (2006). The effect of adding lateral interactions is reported in Fig. 6A3. The global time course of the signal is largely improved thanks to lateral interactions introduction, resulting in a very close correlation between the model and the experimental signals. The transient onset and offset are very close to the experimental one (the rising time constant is 34 ms for the model vs. 35 ms for the experiment) and the model response was much less phasic, in accordance with the experimental data (Fig. 6B3). Interestingly, similar tiny phasic component at the beginning of the response is visible in the experimental and model responses. What happens in this condition is that the tonic component of the global response is boosted by the late lateral component that gradually feeds the modeled column (blue curve in Fig. 6E). The resulting dynamics (red curve in Fig. 6E) has therefore a residual phasic component that originates from the local integration (black curve in Fig. 6E).

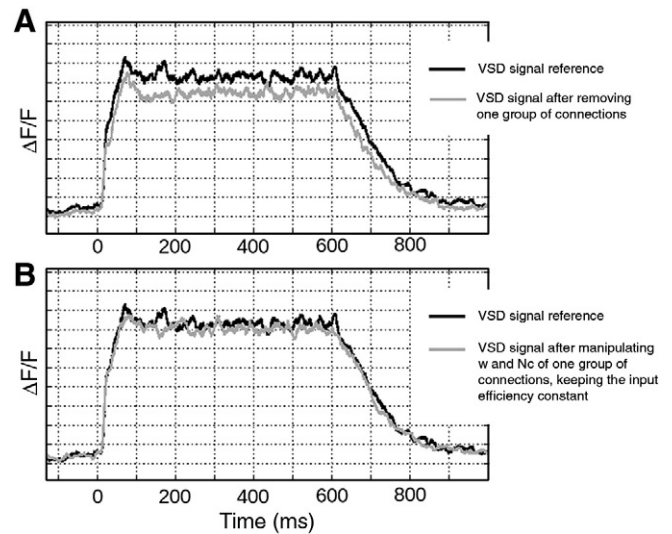


Fig. 7. Model tolerance: analysis of the synaptic weight (w) and the connections number (Nc) parameters. A: temporal evolution of the VSD signal before (black curve) and after (gray curve) removing one group of connections ($W_{SP2 \rightarrow LP5} = 0$). B: temporal evolution of the VSD signal before (black curve) and after (gray curve) applying $W_{SP2 \rightarrow LP5} / 2$ and $Nc_{SP2 \rightarrow LP5} * 2$. The input efficiency being kept constant, the two curves can be superposed.

Note that we verified that the lateral interactions introduction did not change the input–output functions for the spiking rate and the membrane potential of the neurons (see Figs. 4B,E).

Model stability

The model stability was tested by manipulating all the parameters previously quoted, regarding their responsiveness. In order to prove the relevance of the model, it is important to verify that the model is stable to small variations of the parameters and sensitive to larger variations. For example, we studied in details two important parameters of the local network: the synaptic weights (w) and the number (Nc) of connections. Two main tests are reported in Fig. 7. The first one (left panel) shows the sensitivity of the model when removing one group of connections of the network. The second one (right panel) shows that manipulating the synaptic weight (w) and the connections number (Nc) parameters, while keeping the input efficiency constant, does not change the result, as expected.

Several other numerical tests have been issued allowing to verify the numerical stability of the result with respect to small variations of parameters values. However, we have also checked that those parameters do change the response for high variations, verifying that their order of magnitude is meaningful, and their introduction not a redundancy.

Quantitative analysis of the VSD signal sources

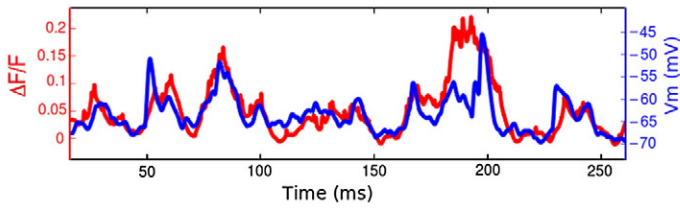
We simulated the VSD signal in term of relative fluorescence by taking relative variations of fluorescence (ΔF) compared to the resting level (F) observed at rest, similar to real experimental conditions.

Correlating the various compartments with the global population signal

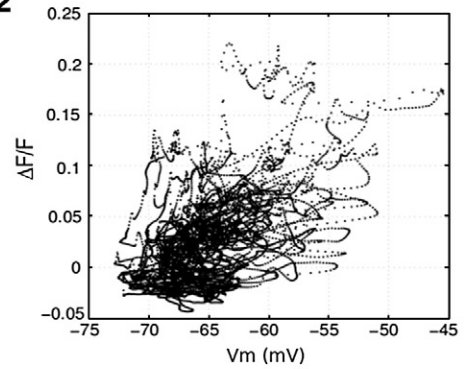
Petersen et al. (2003) and Contreras and Palmer (2003) showed that the VSD signal and the membrane potential fluctuations of a single cell are strongly correlated. Here, we first verify that such a correlation is also observed on our model. We then systematically inspected which compartments and which activity type (subthreshold vs. spiking rate) are at the origin of the time course fluctuations of the global VSD signal.

If we superimpose the dynamics of the model VSD signal to one local membrane potential response of one compartment of the model

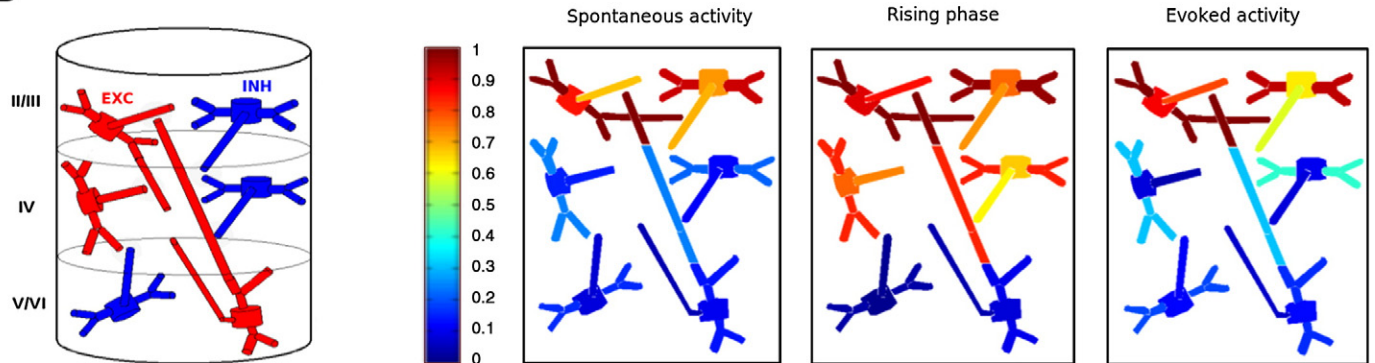
A1



A2



B



C

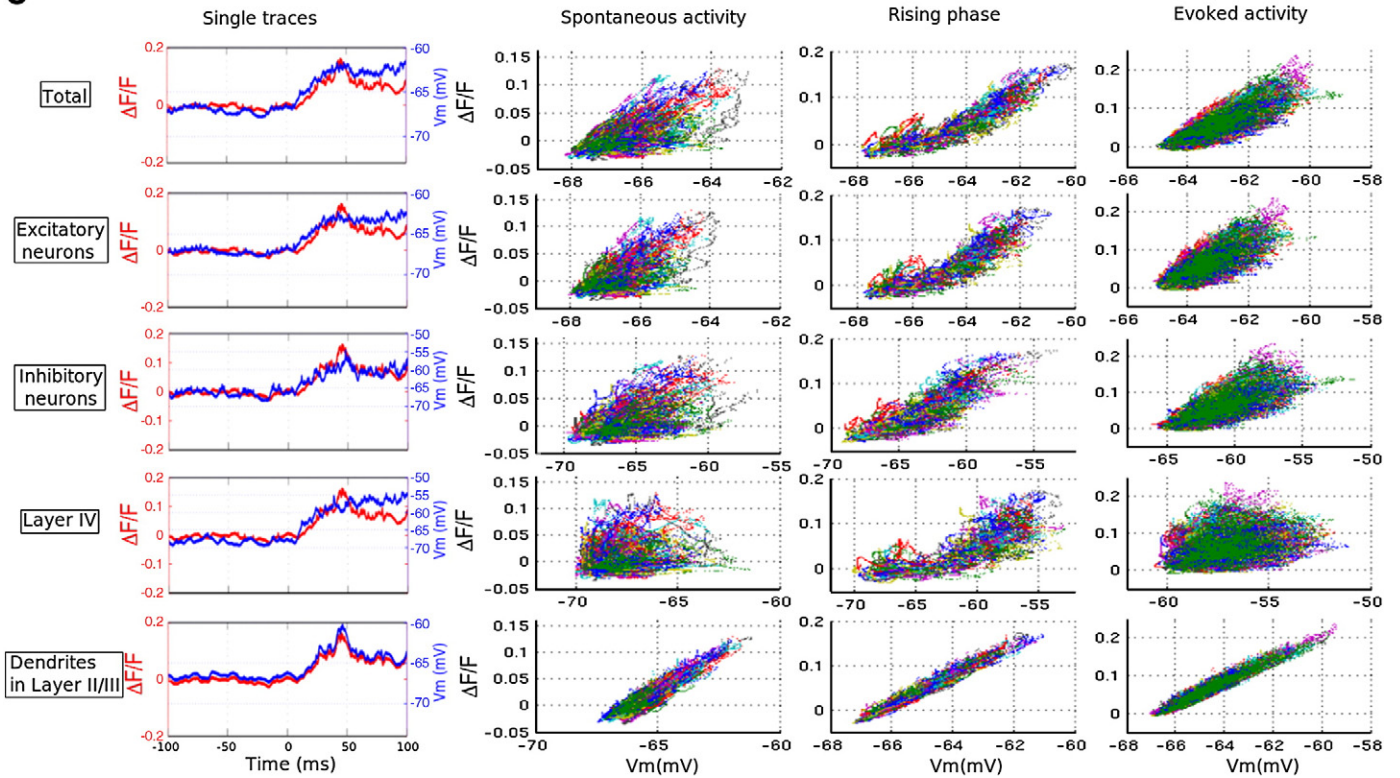


Fig. 8. Correlating membrane potential fluctuations with VSDI global signal. A1: individual membrane potential response (blue trace), superimposed to the modeled VSD signal (red trace, one trial). A2: from A1, the VSD signal is plotted as a function of changes in membrane potential of the individual neuron. B: graphical representation of the correlation between the VSD signal and the membrane potential of each compartments as a function of time for an input frequency of 130 hz. Each frame represents a period of time (in milliseconds). [−200 to −20]: Spontaneous activity. [0 to 50]: Rising phase (time 0 corresponds to the stimulation onset). [50 to 500]: Evoked activity. C: trial to trial correlation analysis between the VSD signal and the membrane potential of five specific contributions (total, excitatory neurons, inhibitory neurons, layer IV and dendrites in layer V).

(Fig. 8A1), we observe that the VSD signal and the membrane potential changes of a single cell are correlated (Fig. 8A2). If we then plot the VSD signal as a function of the spike rate of a population of

single cells (Fig. 9A1), the correlation is only apparent at the transient onset and offset (input-related signal), but high frequency modulation (noise on the plateau) is not correlated. This result qualitatively

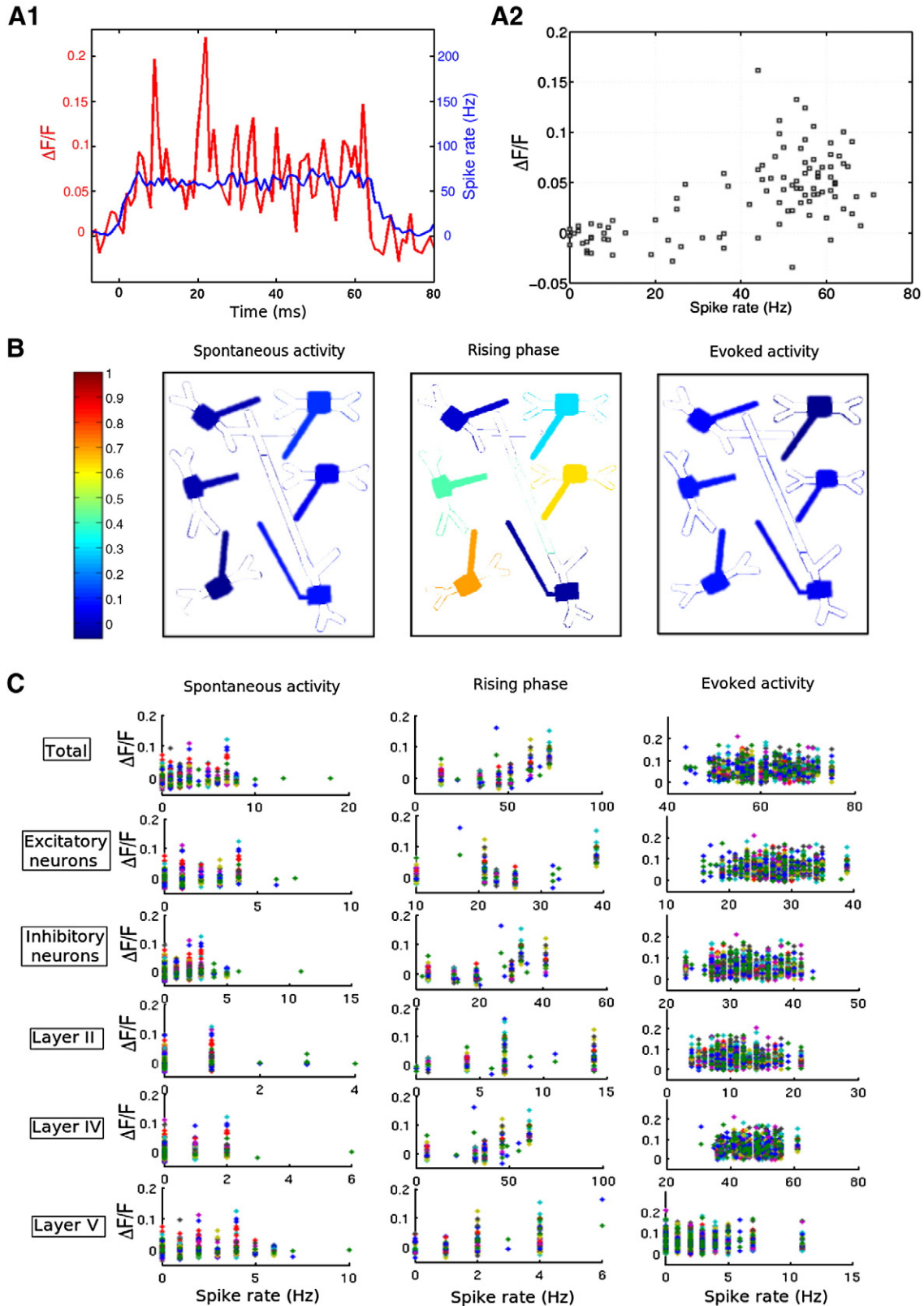


Fig. 9. Correlating spiking rate with VSDI global signal. A1: post stimulus time histogram constructed over the entire column (blue), giving spike counts per bin (10 ms), superimposed to the modeled VSD signal (red), which was binned at the same value. A2: the VSD signal plotted as a function of changes in spike rate of an individual neuron. B: graphical representation of the correlation between the VSD signal and the spike rate of excitatory and inhibitory neurons (somas and axons) in each layer. Same frames decomposition as previously used. C: trial to trial correlation analysis between the VSD signal and the spike rate of six specific contributions (total, excitatory neurons, inhibitory neurons, layer II, layer IV and layer V).

confirms that the VSD signal changes are principally arising from synaptic membrane potential fluctuations.

In order to quantify the relationship between the VSD population signal and both the membrane potential and the spike rate of neuronal elements, we made a correlation study and quantitatively explored the question with our model by looking at each compartment independently. Fig. 8B (resp. Fig. 9B) shows a frame sequence of our cortical column depicting the temporal evolution of the correlation coefficients (or r^2 coefficients) between the membrane potential (resp. the spike rate) of each single compartment and the total VSD signal. Each frame represents a different period of time (in milliseconds): The spontaneous activity (i.e. when no thalamic input is applied) corresponds to the interval $[-200; -20]$. The rising phase corresponds to the interval $[0; 50]$, time 0 is the time of the stimulation onset. Finally, the evoked or sustained activity (i.e. when the thalamic inputs are applied) corresponds to the interval $[50; 500]$. During spontaneous and evoked activity, as the correlations were very stable over time, we averaged over the whole time period. Centered on the rising phase of the response, this representation provides a direct comparison of the correlations between on-going and evoked activity. The trial-to-trial analysis for five (resp. six) specific components is reported in Fig. 8C (resp. Fig. 9C).

Three main results emerge from this correlation study, either concerning input-related changes or high frequencies fluctuations of the signal: (1) the VSD signal is much more correlated with membrane potential than with spikes. The spiking activity of pyramidal neurons in layer II globally explains 2% of the VSD variance, whereas membrane potential of pyramidal neurons in layer II explains 78%. (2) Not surprisingly (see the signal computation part in [Material and methods](#)), the VSD signal is mostly correlated with membrane potential of dendrites in superficial layers (last row in Fig. 8C). The maximal correlation coefficient that we obtained for all compartments, signal and time period was 0.96 for the rising phase of superficial layers depolarization. (3) At the stimulation onset, the correlation between the VSD signal and membrane potential of compartments in layer IV largely increases (from 0.13 to 0.72), the same being true for spiking activity (from 0.02 to 0.52). The latter result is clearly visible in the rising phase frame in Figs. 8B and 9B, and also in the trial-to-trial analysis of Fig. 8C (fourth row), where the best correlation between VSD signals and layer IV membrane potential is found at the rising phase, i.e. the phase occurring at the stimulation onset delineating spontaneous activity from the evoked activity. This increase is due to the thalamic input providing a strong and local input in layer IV, thereby increasing temporarily the correlation with the VSD signal.

Three other results are also interesting to notice: (4) on-going and evoked activities present almost the same correlation coefficients (Figs. 8B, 9B). (5) Excitatory and inhibitory neurons show very similar correlation with the VSD signal. Lastly, (6) spiking activity of inhibitory neurons are more correlated to the VSD signal than excitatory neurons ($r^2=0.3$ for inhibitory neurons in layer II, in comparison to 0.015 for respective excitatory neurons).

We therefore observe that there are dynamic changes of compartment correlations to the global VSD signal at a given thalamic input strength. Note that we ran similar correlation studies with the implementation of the synaptic depression parameter and all our results did not change qualitatively. However, as we previously mentioned, the balance between activity levels in these various compartments will change when the input strength varies. We will now therefore inspect how the activity level affects the different contributions to the VSD global signal.

Contributions to the VSD signal when increasing the level of input activity

To investigate how changing the input frequency can affect the contribution of the various compartments to the population signal, we reproduced another VSDI experiment where the stimulus contrast was

gradually increased (Reynaud et al., 2007, drifting sine-wave gratings presented at seven different contrasts for 600 ms) by computing the temporal evolution of the total VSD signal for seven different thalamic rates (Figs. 10A,B). The set of modeled VSD responses are very close to that of experimental signals at plateau values. The total VSD signal, averaged during 600 ms, is plotted as a function of input rate to be compared with the experimental contrast response function (Figs. 10D,E). This quantitative representation illustrates that the experimental and the model curves indeed have a very similar shape, both fitted by Naka–Rushton function. Our global columnar activation is therefore behaving very closely to the biological column recorded experimentally, except that the input frequency range was not realistic. We then ran the same experiment with the synaptic depression term (Figs. 10C,F), and found a similar behavior, although scaled down to a more realistic input rate and with clearer saturation at high input rate. However, note that, for both simulations, there is a difference in the VSD time course. Experimentally, it is interesting to observe that, in response to a small drifting grating, the experimental VSD (Fig. 10A) is slower than the one measured in response to a static Gaussian luminance stimulus (Fig. 6).

Following the previous formula (Eq. (4)), we can now decompose the VSD signal in its different contributions: excitation, inhibition, somas, axons, dendrites, layer II, layer IV and layer V, and see how their participation to the global signal changes for different levels of input activity. Here we use our model to quantitatively predict the different contributions of the VSD signal, as a function of thalamic increasing input (Fig. 11). For all contributions, we computed the ratios as the amount of VSD signal from one compartment divided by the total VSD signal.

First, we looked at the relative contribution of excitation vs inhibition (Fig. 11A). Globally, excitatory cells are responsible for 83% of the total VSD response, and inhibitory cells participation represents 17% of the VSD signal. The ratio between inhibition and excitation (see squares, right panel) shows that inhibition contribution increases with input rate, about 2.5% from low to high levels of activity. The proportion of inhibitory cell contribution is less than the predicted on the sole basis of activity level and proportion of cellular types, demonstrating the utility of using such a model (see [Discussion](#)). Indeed, if one simply inspects what is the contribution of inhibition when decomposed at the level of dendrites soma and axons (Fig. 12A), we noticed that inhibitory dendrites contribute more than axons and somas. This might be caused by (i) spike thresholding that occurs at the soma, (ii) small spike width of inhibitory cells that minors the inhibitory spiking contribution, and (iii) inhibition that shunts membrane potential at the soma and not at the dendrites.

We then investigate whether the post-synaptic activity contributes differently than spiking activity (Fig. 11B). Globally, 77% of the optical signal comes from dendritic post-synaptic activity. The ratio between axonic and dendritic activity is decreasing with input rate, but weakly, suggesting that synaptic activity is even stronger at high level of activity (see squares, right panel). We attribute this increase in the fact that subthreshold PSPs at dendritic locations are not thresholded by spike generation, whereas spiking activity saturates at high level of activity. In other words, PSPs size continues to increase whereas spiking activity reaches a saturation plateau (see Fig. 12B for an illustration).

What is the participation of cells belonging to deep layers in the global signal (Fig. 11C)? As expected, the optical signal mostly originates from layers II/III neurons (81%), but, the model shows that 19% of the signal in layer II/III comes from the superficial dendrites of deep layer neurons (layers IV and V). The ratio between deep and superficial neurons shows a tiny increase of deep layers contribution with input rate (see squares, right panel).

Finally, we quantified whether the proportion of activity arising from the local connectivity changes with input rate (Fig. 11D). The ratio is largely decreasing when increasing the input rate, showing that local activity contribution decreases with input rate. At low input, the signal is only coming from local recurrent activity (100%) and

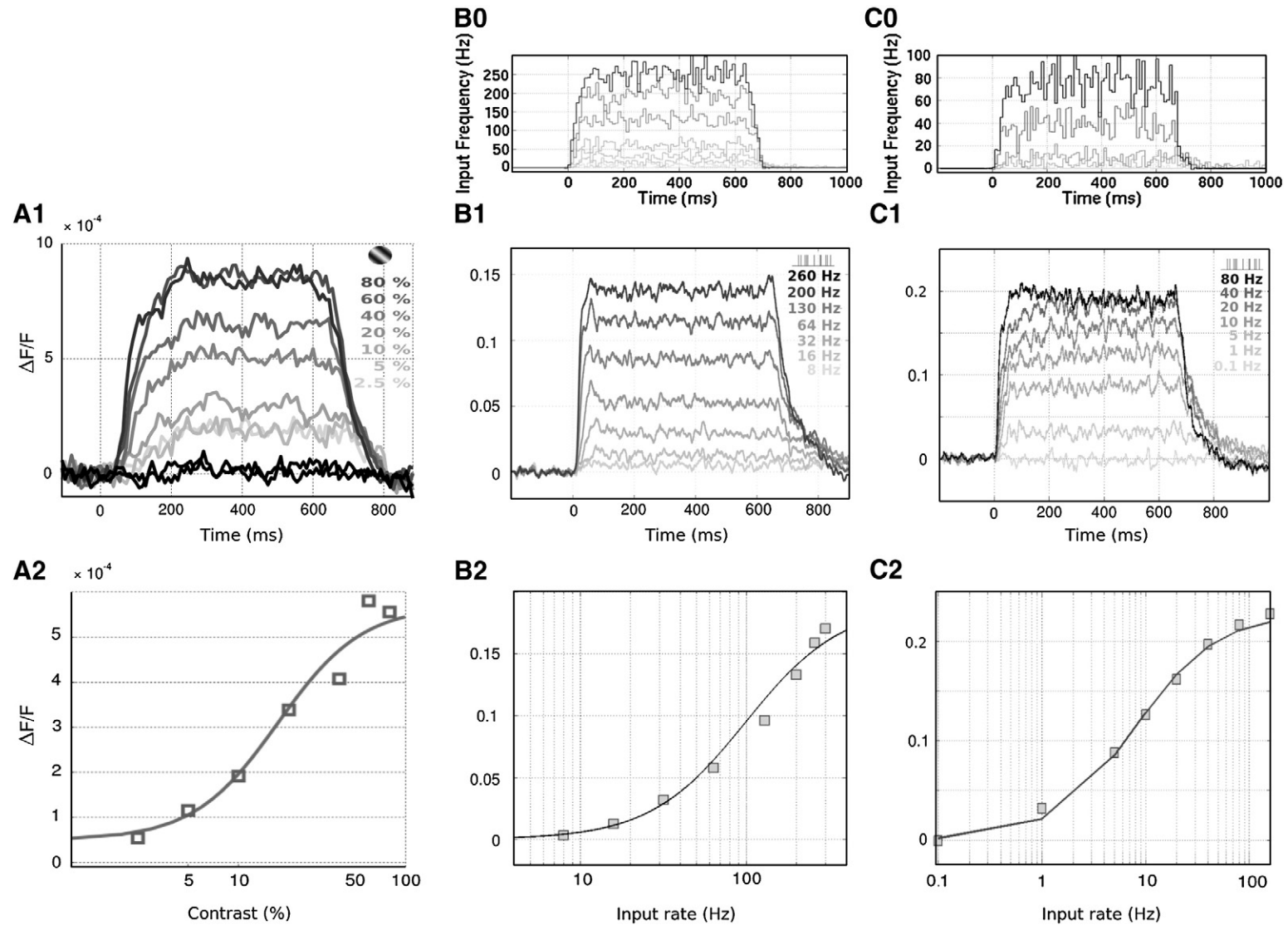


Fig. 10. Total VSD signal computed from the entire network (local connectivity + lateral interactions (B panel) and local connectivity + lateral interactions + synaptic depression (C panel)) and plotted as a function of thalamic input rate. extbA: VSDI experiment on monkey using VSDI (Reynaud et al., 2007). The experimental VSD signal is plotted as a function of time and in response to different input contrasts. In this experiment, monkey had to fixate a central dot while drifting sine-wave gratings are presented behind a circular aperture (2 dia) for 600 ms. Target was presented at 7 different contrasts: 2.5, 5, 10, 20, 40, 60 and 80%. B, C: model, each response is the average of the VSD signal for 100 repetitions of a given input rate.

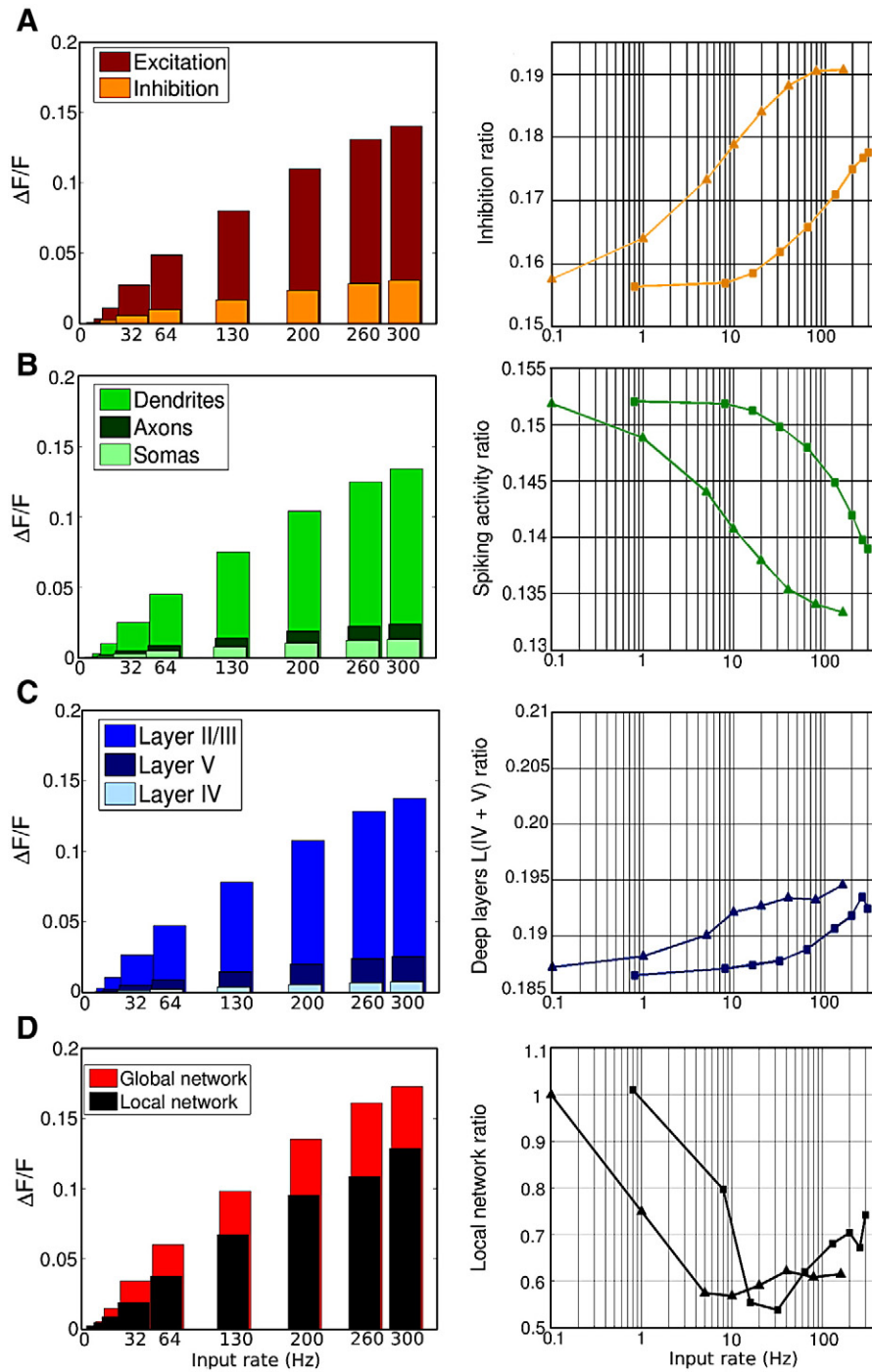


Fig. 11. VSD responses in function of thalamic input rate showing quantitatively the different contributions of the VSD signal when increasing the level of input activity. The rationale between the different contributions are plotted in the right column. Squares are the contributions from our full model without synaptic depression, whereas triangles for the full model with synaptic depression. A: excitation and inhibition contributions. The ratio inhibition/excitation shows that inhibition contribution lightly increases with input rate. B: somas, axons and dendrites contributions. The ratio between axonic and dendritic activity is weakly decreasing with input rate. C: layers contributions. Deep layers contribution weakly increases with input rate, as shown by the ratio in the right. D: local vs. global contributions. The ratio between local and global activity shows that local activity contribution decreases when increasing the input activity.

decreases to 60% for higher input frequency (see squares right panel). The rest of the VSD global signal is coming from inputs from lateral connectivity that contribute more and more for increasing input rate.

Qualitatively, none of these results were affected by the addition of the synaptic depression parameter in our model (triangles in right panel). Input rate similarly increased the contribution of inhibition, decrease spiking activity participation, did not affect much lower layer participation, and decrease the overall contribution of local network

to the global VSD signal. The only main effect was a global scale down of the effect to more realistic thalamic input rates. Thereby, the model quantifies the fact that 80% of the VSD signal originates from dendritic activity of excitatory neurons in superficial layers. However, inhibitory cells, spiking activity and deep layers represent about 20% of the total that is non-negligible. The VSD signal should be considered as a dynamic signal whose constitution depends on time and activity levels.

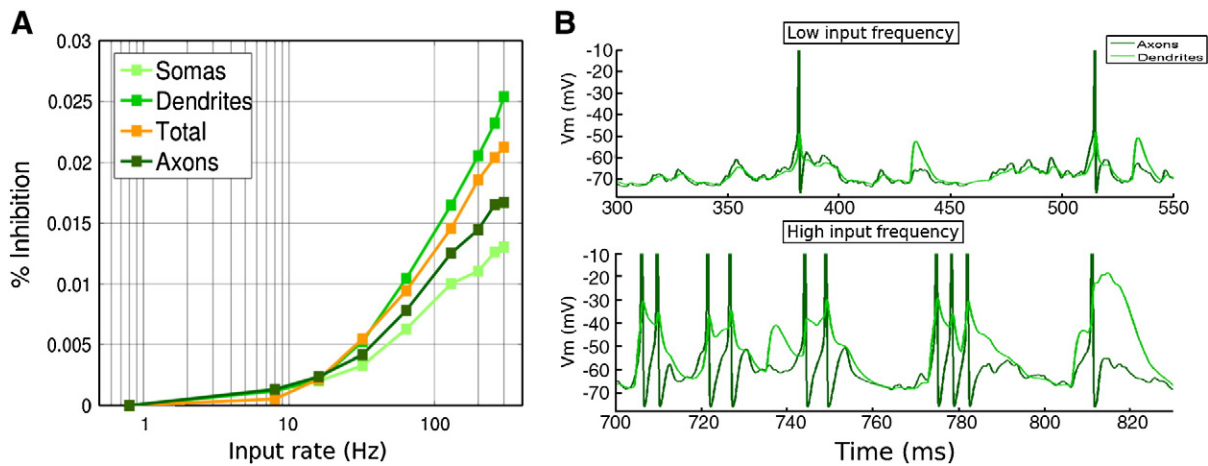


Fig. 12. Decomposition of the inhibition contribution. A: contributions of the different part of the neuron (somas, axons, and dendrites) to the inhibition contribution. B: dendritic and axonic activities of an individual neuron in layer II/III for low vs. high level of input activity.

Discussion

Summary and major results

The purpose of this paper was to better understand what exactly the voltage-sensitive dye imaging signal measures. This question is indeed difficult to resolve at the physiological level since the signal is multi-component: the dye reflects the dynamics of the membrane potential of all membranes in the neuronal tissue, including all layers of the circuitry, all cell types (excitatory, inhibitory, and glial) and all neuronal compartments (somas, axons, and dendrites). However, no other model has been built in the literature to quantitatively examine all these different contributions as well as the spiking activity of the network and the origin of the VSD signal remain unresolved (see (Chemla and Chavane, 2010), for a review on the subject). Experimentally, this quantification is very difficult to realize *in vitro* and quasi impossible *in vivo*. Qualitatively, it is assumed that the VSD signal in a given pixel mostly originates from the dendrites of upper layer cortical cells, and therefore, mainly reflects dendritic activity (Grinvald and Hildesheim, 2004). To perform a quantitative analysis taking into account all these details, we used a realistic biophysical cortical column model, at a mesoscopic scale, with biological and electrical neural parameters of the laminar cortical structure. VSD signal was computed with a linear formula taking into account each compartment level of depolarization, membrane surface and staining. We validated the model by comparing simulated and experimental VSD signals.

The model predicts the different contributions of this signal. As expected, the VSD signal mainly reflects dendritic activity (77% of excitatory neurons (83%) in superficial layers (81%). However, inhibitory cells (17%), spiking activity (23%) and deep layers (19%) represent about 20% of the total signal that is non-negligible and should be taken into account in the interpretation of the VSD signal. Importantly, the contributions of these compartments change as a function of the general level of input activity, suggesting that the VSD signal has a dynamical multi-component origin. This result is reinforced by a correlation analysis that unveils a stronger involvement of layer IV neurons and inhibitory spiking activity during transient input (onset of the stimulus for example).

Dissecting the VSD signal, and back

Our model's results suggest that the contribution of inhibitory cells to the global VSD signal increases with increasing input, from 15.6% to 17.8%. Could these results be predicted just on the basis of numbers the model was fed with? To infer the overall inhibitory contribution, one

should take into account the fact that inhibitory cells are four times less numerous than excitatory cells, but also the cellular morphology differences between stellate and pyramidal neurons (larger membrane surface). In our model, following Table 1, the membrane surface integrated over all inhibitory compartments represents only 12% of total membrane surface. This is lower than our observation and may be explained if now one takes into account activity level. Indeed, inhibitory cells are following the input with a higher spiking rate and subthreshold depolarization (see Fig. 4). However, a deeper look at these values, tuned to fit experimental observations (Contreras and Palmer (2003)), actually shows that the ratio of inhibitory spiking activity over the sum of excitatory and inhibitory spiking rate does not change with increasing input rate (stays around 77%). At the level of membrane potential depolarization, the ratio is even decreasing from 75% to 62%.

This departs from our model prediction that inhibitory contribution actually increases with input rate. Deviation from such simple linear predictions originates from the multiple non-linearities that actually control the model behavior, and supposedly the actual biological network. For example, non-linearities exist in the conductance-based inhibition and spike generation that constraint membrane potential dynamics at the somatic level. When we decompose the contribution of inhibition at the level of dendrites, soma and axons (Fig. 12A), we indeed observe that the spike thresholding and spike width (smaller for inhibitory cells) strongly reduce the inhibitory contribution. These observations demonstrate the need of a detailed biophysical model that takes into account all these details to make an exact estimation of the relative contribution of inhibition and excitation.

Similarly, the relative contribution of subthreshold vs. spiking activity is difficult to predict a priori. One would also have to take into account on one hand, linear parameters such as the smaller depolarization area under spiking activity, but also the smaller surface of axons compared to dendritic trees. On the other hand, non-linear interaction parameters as mentioned above are also present. Our model predicts that the overall contribution of pure spiking activity (on axons) to VSDI is of the order of 14%. Importantly, it also predicts that this contribution will decrease with input strength from 15.2% to 13.8%. We explain this decrease by the major contribution to VSD signal of synaptic activity in dendritic arborization of upper layers that is not constrained by membrane potential clamping occurring in the soma because of spikes or inhibitory conductances (Fig. 12B).

An important additional information is coming from the studies of temporal correlation between different compartments and the global VSD signal. The high frequency variation of the global VSD signal is mostly due to dendritic activity. Importantly, the global VSD signal variance is equally well explained for excitatory and inhibitory neurons, and for spontaneous

and evoked activity. This correlation study also informed us that, during the response transient phase, the VSD signal becomes strongly correlated to the activity of layer IV neurons (in accordance with [Bush and Priebe, 1998](#)) and also to the spiking activity of inhibitory neurons. This brings us to the conclusion that VSD transient and sustained phases have different origins. It may have important consequence when interpreting the signal, especially regarding more complex natural visual stimuli, which contain many transients ([Kremkow, 2009](#)).

These results suggest that the relative contribution of all compartments are not only a function of input strength, but also of time, transient and sustained input having different impacts on the recurrent cortical column ([Douglas and Martin, 1991](#); [Borg-Graham et al., 1998](#); [Muller et al., 2001](#); [Crowder et al., 2008](#); [Stoelzel et al., 2008](#)). More precisely, it is interesting to note that the synchrony of thalamic input generates a strong transient in the VSD signal that is attenuated by onset asynchronies and the presence of horizontal inputs ([Fig. 6](#)). However, a small phasic component is always present in the model and also in the observed response. This is strongly reminiscent of the so-called “notch” component introduced by [Sharon and Grinvald \(2002\)](#), identified by these authors as “a small transient drop in the rate at which the evoked response increased (...) which we term the evoked deceleration–acceleration (DA) notch”. Our model suggests that this notch is the residual of a phasic response to stimulus onset, hidden under a large horizontal convergence of input from neighboring columns. One prediction of our model is therefore that the time constant of VSD signal is slowed down by horizontal converging input, that contributes more and more with time ([Fig. 6E](#)) and with increasing contrast ([Fig. 11D](#)). The VSD response is thus dynamic, from local to global activity with a time constant of about 100 ms ([Fig. 6E](#)).

When we look at the contribution of lower layers, our result shows that, even if the dye gradient we chose is favoring dramatically upper layers (95%), cells in layer IV or layers V/VI contribute more than expected by the dye gradient. This is because activity in superficial layers is also provided by layers V and VI pyramidal neurons, whose apical dendrites do reach superficial layers ([Thomson and Bannister, 2003](#)). Because of the presence, in upper layers, of dendrites of lower layers, the contribution is four times more than what the gradient imposed (19% instead of 5%). In this model we used the distribution of fluorescence intensity estimated by [Lippert et al. \(2007\)](#) who concluded that the VSD signal mostly originates from superficial layers (I–III). One can question how much the dye gradient indeed interferes with our results. The only quantitative data on dye gradient comes from experiments on the rodent model by [Kleinfeld and Delaney \(1996\)](#), [Petersen et al. \(2003\)](#) and [Lippert et al. \(2007\)](#). Following the staining depth of the dye, the authors concluded that the VSD signals originate from superficial cortical layers I–III. Their staining procedures on rat barrel and visual cortices however differ from that used on higher mammal species like monkey. We have therefore tested other ad-hoc values of dye gradient. When choosing striking different values ($\lambda^2=0.6$, $\lambda^4=0.3$ and $\lambda^5=0.1$), it appears that neither the relative contributions of the different components (excitation, inhibition, spiking activity, and synaptic activity), nor their global evolution when increasing the level of input activity, have changed. As expected, the relative contribution of the different layers has obviously changed. For these values, 45% of the total signal comes from neurons in layer II/III, 20% from neurons in layer IV and 35% from neurons in layer V. The latter contribution can be decomposed into more precise quantities: 7% is from dendrites found in layer II/III, but belonging to layer V pyramidal cells, 20% is from dendrites found in layer IV but also belonging to layer V pyramidal cells and the last 8% is actually from neurons in layer V.

Once we have shown that the VSD signal is multi-composite and that the various contributions are a function of time and contrast, we may wonder whether we could solve the inverse problem? In other words, from the actual VSD signal, would it be possible to predict the contribution of the various components? This paper showed that four

unknown variables (contributions of the different compartments) are a function of two known variables (contrast and time here). Ideally, one would like to find two more known variables that would control the unknowns differentially. From there, theoretically at least, we could reconstruct the relative contributions of all these variables from the global VSD signal. However, for that purpose, the model would need to be improved drastically to represent more functional parameters. Indeed, adding the notion of receptive field encoding orientation and position parameters could lead to a well-posed reverse problem (assuming linear equations), with four unknowns and four variable parameters (contrast, time, orientation and position). Therefore, for one given pixel, these four parameters could be varied in real VSDI, leading to a set of experimental recordings that could be used to adjust our model for reverse-engineering. This, ideally, could allow us to find back the origin of the signal. We therefore wish to improve our model in the future to represent more functional parameter spaces in order to better constrain the various compartments participation to the global VSD signal.

The role of synaptic depression

Inhibition within our cortical column was not enough *per se* to control and dampen the thalamic excitatory input. This surprised us as we tuned our model to incorporate realistic inhibition, with important properties such as a much higher output rate than excitatory neurons, and a shunting effect on post-synaptic somatic compartments. Despite these important parameters, and unlike contrast response function of V1 neurons, our modeled neurons did not completely saturate at high input rates (see [Fig. 4](#)). We therefore decided to introduce synaptic depression at the thalamo-cortical synapses, as it was suggested to play an important role in contrast gain control mechanisms ([Carandini et al., 2002](#)). This term was indeed enough for scaling down the input rate to more realistic regime for which saturation of cortical neurons were observed. We controlled how this new parameter affected our main results. Importantly, except from scaling down all these effects for realistic input rate, synaptic depression did not make any qualitative changes in our correlation and contribution studies. We therefore conclude that this parameter is fundamental for adjusting the operating range of the cortical column, without affecting the contribution of the various neuronal compartments to the global VSD signal.

Is the biophysical model detailed enough?

The present work shows that there was a need to develop a model at an intermediate scale between the so-called microscopic and mesoscopic scales. This simple compartmental model (only 8 to 10 compartments per neurons) is detailed enough in order to simulate and better understand which part of the neuron is involved in the generation of the dye signal, while it is simple enough to both derive tractable numerical simulations, and (even more important) do not over-parametrize the problem.

Although we modeled in details only a unique cortical column of $50 \times 50 \mu\text{m}^2$ lateral area, we reproduced the activity of an entire hypercolumn of about $750 \mu\text{m}$ by simulating continuous background activity and lateral connectivity between neighboring cortical columns. In order to calibrate neuron responses, we used optimization algorithms to select model parameters in accordance with experimental observations, both at single cell ([Nowak et al., 2003](#)) and fully connected network ([Contreras and Palmer, 2003](#)). By doing a stability analysis, we verified the reliability of the model with respect to small and large variations in parameter values. The model was built step by step, i.e. single neurons, local network, background activity and then lateral interactions, in order to control precisely the action of each parameter and, as explained above, to find the minimal number of parameters required to reliably reproduce the VSD signal, as obtained experimentally using VSDI on monkey primary visual cortex.

A more detailed model of the neuron would have allowed us to play with a larger number of parameters, maybe allowing to encounter for “any” signal, but the related interpretation would have been subject to caution. At this stage, a potential perspective and improvement for the model would be the introduction of new nonlinearities and test how much they affect our results. For example, we could introduce synaptic depression at thalamo-cortical synapses, suggested to play an important role in contrast gain control mechanisms (Carandini et al., 2002). However, our position here was to use the *minimal* model which could integrate the data available in the literature, and which was relevant for the addressed questions.

Another perspective is to increase the model size towards a larger network, accounting for columnar cortical architecture such as orientation maps. With such a model, new questions could be addressed, for example, trying to explain why VSDI signal has such a poor orientation selectivity (Sharon and Grinvald, 2002). Indeed, the response of any orientation column to a stimulus oriented orthogonal to the preferred direction is about 80% of the maximum response (Grinvald et al., 1999). In comparison, for the orthogonal stimulus, neurons have spiking response that is nearly null (5% of the maximum) and subthreshold activation a bit more than 20% of the maximum response (Monier et al., 2003). Therefore, a model at this stage would help understanding where the remaining 60% of activation in the global VSD signal is coming from. To enlarge the model, a large amount of improvements would be needed. For example, a higher degree of specific lateral interactions among distant columns of varying orientation selectivity should be implemented. Such improvement of the model would then allow us to generate a receptive field structure for each of our cells. This would have a high interest as we could specifically study the impact of subthreshold waves of activity converging from the periphery of receptive fields on VSDI signals (Bringuier et al., 1999): so far, we have only modeled the horizontal waves with convergent random spike trains. Furthermore, this will allow us to study more complex dynamics of stimuli whose spatial phase is dynamically changing.

At the implementation level, enlarging the model would require a higher order of magnitude of calculation, which is easily realizable on a cluster (though this is far beyond the present work), the underlying NEURON software having this parallelization capability. Another track would be to make our model interact with a mesoscopic model of the V1 laminar network (i.e. a model considering a large network of punctual spiking neurons), in order to simulate the present pixelic column with more realistic inputs than pure stochastic inputs. At the implementation level, this requires the capability to have several neural simulators interoperable (i.e. a meta-simulator), which is realizable nowadays with the PyNN meta-simulation platform (Davison et al., 2009), though the present software tools are still at the development stage.

Inadequacies with experimental data and limitations

Although the model accurately reproduces the VSD signal, there are some experimental results, listed below, with which it is not consistent. However, these discrepancies are mainly due to the minimalism of the model.

The present model does not have a realistic representation of the LGN drive. Indeed, in the present study, inputs signals from the thalamus into neurons in layer IV are simulated by applying random spike trains of a given averaged discharge frequency. This solution is a first good approximation and was good enough to reproduce experiments with static stimuli. However, for a more complex stimulation (Fig. 10), i.e. drifting sinusoidal grating, the model could not reproduce the slower time course observed experimentally. With the model such as the one presented here, we could not find a parametric solution that would slow down the response time course to fit the experimental observation. These conditions were good enough to study the contrast response

function at steady-state levels though. However, this discrepancy suggests that it would be necessary for future studies to add new functionalities that would allow to improve the realism of the thalamo-cortical integration.

Improvements could be achieved on two aspects of our model. One important point is that thalamic input rate should be modulated by a phasico-tonic envelope such as implemented in Gazeres et al. (1998) model of X-non-lagged cells, in order to reveal the dynamics of the initial ON transient in the VSD signal (Slovin et al., 2002; Sharon and Grinvald, 2002; Sharon et al., 2007; Ahmed et al., 2008; Lippert et al., 2007; Meirovithz et al., 2009). Moreover, the input should not only incorporate X-non-lagged type as we did in the model, but the full response dynamic should also be modulated by Y and lagged thalamic inputs (Hartveit and Heggelund, 1992, 1994). The convergence of such an input mixture will most probably affect the global time course of our model. A second point is that neurons in our cortical column are devoid of receptive field structure (i.e. they are thus considered to be stimulated in their center, not in their periphery) and hence cannot capture the complex dynamic of a stimulus whose phase is dynamically changing. All thalamic inputs will be integrated similarly for all neurons. We believe that this is the main origin of our discrepant time-courses. Drifting grating will affect differently the dynamical response of neurons depending on their receptive field structure (Movshon et al. (1978a,b), Skottun et al. (1991), Contreras and Palmer (2003)). We therefore believe that the phase-dependent and independent responses summed over the whole column will slow down the global VSDI time course. However, to implement this new functionality a significant enlargement of the model size should be achieved. To take into account differences in receptive field position, orientation and scatter (Albus, 1975a,b), a hypercolumn size should be reached at least. This will be the direction of future development of our model. Interestingly, using such a model enlargement, new questions regarding the origin of the VSDI signal could be tackled, such as the ones described above.

The present model contains no detailed representation of the long-range lateral connections, nor does it contain any NMDA channels. In comparison, the large scale VSD cortical model of Rangan et al. (2005), although restricted to a single layer and to point neurons, does contain a realistic number of ion channels and extends laterally over several mm² (see Chemla and Chavane, 2010, for a review on VSD models). Spiking neurons over large cortical distances are connected by long-range connections through AMPA and NMDA synapses. The authors claimed that these slow NMDA conductances allow to capture the *in vivo* behavior of coherent spontaneous activity. These authors showed that a very small ratio of NMDA contribution (5%) is enough to provide the desired features and turn the cortex into a regime that they called “intermittent desuppression”. According to this study, without NMDA receptors, cell's spontaneous activity will not be consistent with *in vivo* experimental observations in the cat visual cortex anymore (Cai et al., 2005). To check whether NMDA conductance would affect spontaneous level of activity and our signal dynamics, we therefore made control simulations with NMDA conductance at long-range synapses (see Supplementary Fig. 2), according to the description of Rangan et al. (2005) and Cai et al. (2005). At the global level, this new parameter did not affect significantly the VSDI time course ($\tau = 32$ ms) or the fractional signal ($\Delta F/F = 0.22$ for an input rate of 80 Hz). In comparison to Rangan et al. (2005) and Cai et al. (2005) models, though, our model was not large enough to capture dynamic propagation of horizontal activity for which NMDA conductance might reveal to have a more fundamental role.

Conclusion

Our aim in the present study was to raise awareness on the dynamic origin of the VSDI signal. On one hand, our model enables to have a realistic estimation of the relative contributions of the various

components constituting the global signal. On the other hand, it revealed that the compositionality of the signal is highly dynamic and depends on input strength and transience. We believe that these global observations will not be affected by improving the microscopic level or enlarging the mesoscopic aspect of the model. Rather, this study is the first attempt to better apprehend this complex signal and should help interpreting and designing VSDI experiments. We hope that further developments of such direct models will allow at one stage to help solve the inverse problem.

Acknowledgments

The authors are indebted to Thierry Vieville for its large contribution both on the model development and the manuscript preparation. They thank Alain Destexhe for providing helpful suggestions in particular regarding the choice of the model parameters. They also thank Ted Carnavale, Michael Hines and Pdraig Gleeson for their help with the simulation softwares. Finally, they thank Guillaume Masson and Alexa Riehle for helpful comments on the manuscript and Alexandre Reynaud for providing them the experimental data.

This work is realized within the scope of the European FACETS integrated project (IST-15879).

Appendix A. Supplementary data

Supplementary data associated with this article can be found, in the online version, at doi:10.1016/j.neuroimage.2010.06.026.

References

- Ahmed, B., Hanazawa, A., Undeman, C., Eriksson, D., Valentiniene, S., Roland, P.E., 2008. Cortical dynamics subserving visual apparent motion. *Cereb. Cortex* 18 (12), 2796–2810.
- Albrecht, D., Hamilton, D., 1982. Striate cortex of monkey and cat: contrast response function. *J. Neurophysiol.* 48 (1), 217–233.
- Albus, K., 1975a. A quantitative study of the projection area of the central and the paracentral visual field in area 17 of the cat. i. the precision of the topography. *Exp. Brain Res.* 24 (2), 159–179.
- Albus, K., 1975b. A quantitative study of the projection area of the central and the paracentral visual field in area 17 of the cat. ii. the spatial organization of the orientation domain. *Exp. Brain Res.* 24 (2), 181–202.
- Alonso, J.-M., Usrey, W., Reid, R.C., 2001. Rules of connectivity between geniculate cells and simple cells in cat primary visual cortex. *J. Neurosci.* 21 (11), 4002–4015.
- Anderson, J., Carandini, M., Ferster, D., 2000. Orientation tuning of input conductance, excitation, and inhibition in cat primary visual cortex. *J. Neurophysiol.* 84 (2), 909–926.
- Binzegger, T., Douglas, R., Martin, K., 2004. A quantitative map of the circuit of cat primary visual cortex. *J. Neurosci.* 24 (39), 8441–8453.
- Borg-Graham, L., Monier, C., Fregnac, Y., 1998. Visual input evokes transient and strong shunting inhibition in visual cortical neurons. *Nature* 393, 369–373.
- Brent, R., 1976. A new algorithm for minimizing a function of several variables without calculating derivatives. Prentice Hall, Englewood Cliffs, NJ, pp. 200–248.
- Bringuiet, V., Chavane, F., Glaeser, L., Fregnac, Y., 1999. Horizontal propagation of visual activity in the synaptic integration field of area 17 neurons. *Science* 283 (5402), 695–699.
- Bush, P., Priebe, N., 1998. Gabaergic inhibitory control of the transient and sustained components of orientation selectivity in a model microcolumn in layer 4 of cat visual cortex. *Neural Comput.* 10 (4), 855–867.
- Bush, P., Sejnowski, T., 1993. Reduced compartmental models of neocortical pyramidal cells. *J. Neurosci. Meth.* 46, 159–166.
- Bush, P., Prince, D., Miller, K., 1999. Increased pyramidal excitability and NMDA conductance can explain posttraumatic epileptogenesis without disinhibition: a model. *J. Neurophysiol.* 82, 1748–1758.
- Buzas, P., Kovacs, K., Ferecsko, A.S., Budd, J.M., Eysel, U.T., Kisvarday, Z.F., 2006. Model-based analysis of excitatory lateral connections in the visual cortex. *J. Comp. Neurol.* 499, 861–881.
- Cai, D., Rangan, A.V., McLaughlin, D.W., 2005. Architectural and synaptic mechanisms underlying coherent spontaneous activity in v1. *Proc. Natl Acad. Sci.* 102 (16), 5868–5873.
- Carandini, M., Heeger, D., Senn, W., 2002. A synaptic explanation of suppression in visual cortex. *J. Neurosci.* 22 (22), 10053–10065.
- Chemla, S., Chavane, F., 2010. Voltage-sensitive dye imaging: technique review and models. *J. Physiol. Paris* 104, 40–50.
- Contreras, D., Palmer, L., 2003. Response to contrast of electrophysiologically defined cell classes in primary visual cortex. *J. Neurosci.* 23 (17), 6936–6945.
- Crowder, N., Hietanen, M., Price, N., Clifford, C., Ibbotson, M., 2008. Dynamic contrast change produces rapid gain control in visual cortex. *J. Physiol.* 586 (Pt 17), 4107–4119.
- Davison, A., Bruderie, D., Eppler, J., Kremkow, J., Muller, E., Pecevski, D., Perrinet, L., Yger, P., 2009. Pynn: a common interface for neuronal network simulators. *Front. Neuroinformatics* 2.
- Destexhe, A., Rudolph, M., Fellous, J., Sejnowski, T., 2001. Fluctuating synaptic conductances recreate in-vivo-like activity in neocortical neurons. *Neuroscience* 107, 13–24.
- Douglas, R., Martin, K., 1991. A functional microcircuit for cat visual cortex. *J. Physiol.* 735–769.
- Douglas, R., Martin, K.A.C., 2004. Neuronal circuit of the neocortex. *Ann. Rev. Neurosci.* 27, 419.
- Fregnac, Y., Monier, C., Chavane, F., Bandot, P., Graham, L., 2003. Shunting inhibition, a silent step in visual cortical computation. *J. Physiol. Paris* 97, 441–451.
- Gazeres, N., Borg-Graham, L., Fregnac, Y., 1998. A model of non-lagged X responses to flashed stimuli in the cat lateral geniculate nucleus. *Vis. Neurosci.*
- Grinvald, A., Hildesheim, R., 2004. VSDI: a new era in functional imaging of cortical dynamics. *Nature* 5, 874–885 URL <http://www.nature.com/reviews/neuro>.
- Grinvald, A., Shoham, D., Shmuel, A., Glaser, D., Vanzetta, I., Shtoyerman, E., Slovlin, H., Arieli, A., 1999. In-vivo optical imaging of cortical architecture and dynamics. In: Windhorst, U., Johansson, H. (Eds.), *Modern Techniques in Neuroscience Research*. Springer Verlag, pp. 893–969.
- Gupta, A., Wang, Y., Markram, H., 2000. Organizing principles for a diversity of gabaergic interneurons and synapses in the neocortex. *Science* 287, 273–278.
- Haeusler, S., Maass, W., 2007. A statistical analysis of information-processing properties of lamina-specific cortical microcircuits models. *Cereb. Cortex* 17, 149–162.
- Hartveit, E., Heggelund, P., 1992. The effect of contrast on the visual response of lagged and nonlagged cells in the cat lateral geniculate nucleus. *Vis. Neurosci.* 9, 515–525.
- Hartveit, E., Heggelund, P., 1994. Response variability of single cells in the dorsal lateral geniculate nucleus of the cat. comparison with retinal input and effect of brain stem stimulation. *J. Neurophysiol.* 72 (3), 1278–1289.
- Hines, M., Carnevale, N., 1997. The neuron simulation environment. *Neural Comput.* 9, 1179–1209.
- Hodgkin, A., Huxley, A., 1952. A quantitative description of membrane current and its application to conduction and excitation in nerve. *J. Physiol.* 117, 500–544.
- Kleinfeld, D., Delaney, K., 1996. Distributed representation of vibrissa movement in the upper layers of somatosensory cortex revealed with voltage-sensitive dyes. *J. Comp. Neurology* 375, 89–108.
- Kremkow, J., 2009. Correlating excitation and inhibition in visual cortical circuits: Functional consequences and biological feasibility. Ph.D. thesis, Université de Aix-Marseille II.
- Lippert, M.T., Takagaki, K., Xu, W., Huang, X., Wu, J.Y., 2007. Methods for voltage-sensitive dye imaging of rat cortical activity with high signal-to-noise ratio. *J. Neurophysiol.* 98, 502–512.
- Markram, H., Wang, Y., Tsodyks, M., 1998. Differential signaling via the same axon of neocortical pyramidal neurons. *Proc. Natl Acad. Sci. USA* 95, 5323–5328.
- Mastrorarde, D., 1987. Two classes of single-input x-cells in cat lateral geniculate nucleus. i. receptive-field properties and classification of cells. *J. Neurophysiol.* 57 (2), 357–380.
- Meirovithz, E., Ayzenshtat, I., Bonneh, Y., Itzhack, R., Werner-Reiss, U., Slovlin, H., 2009. Population response to contextual influences in the primary visual cortex. *Cereb. Cortex* 20 (6), 1293–1304.
- Monier, C., Chavane, F., Baudot, P., Graham, L., Y., F., 2003. Orientation and direction selectivity of synaptic inputs in visual cortical neurons: a diversity of combinations produces spike tuning. *Neuron* 37 (4), 663–680.
- Movshon, J., Thompson, I., Tolhurst, D., 1978a. Receptive field organization of complex cells in the cat's striate cortex. *J. Physiol. (London)* 283, 79–99.
- Movshon, J., Thompson, I., Tolhurst, D., 1978b. Spatial summation in the receptive fields of simple cells in the cat's striate cortex. *J. Physiol. (London)* 283, 53–77.
- Muller, J., Metha, A., Krauskopf, J., Lennie, P., 2001. Information conveyed by onset transients in responses of striate cortical neurons. *J. Neurosci.* 21 (17), 6978–6990.
- Nowak, L.G., Azouz, R., Sanchez-Vives, M.V., Gray, C., McCormick, D., 2003. Electrophysiological classes of cat primary visual cortical neurons in vivo as revealed by quantitative analyses. *J. Neurophysiol.* 89, 1541–1566 URL <http://jn.physiology.org/cgi/content/abstract/89/3/1541>.
- Petersen, C., Grinvald, A., Sakmann, B., 2003. Spatiotemporal dynamics of sensory responses in layer 2/3 of rat barrel cortex measured in vivo by voltage-sensitive dye imaging combined with whole-cell voltage recordings and neuron reconstructions. *J. Neurosci.* 23 (3), 1298–1309.
- Raizada, R., Grossberg, S., 2003. Towards a theory of the laminar architecture of the cerebral cortex: computational clues from the visual system. *Cereb. Cortex* 13, 100–113.
- Rangan, A.V., Cai, D., McLaughlin, D.W., 2005. Modeling the spatiotemporal cortical activity associated with the line-motion illusion in primary visual cortex. *Proc. Natl Acad. Sci.* 102 (52), 18793–18800.
- Reid, R.C., Alonso, J.-M., 1996. The processing and encoding of information in the visual cortex. *Curr. Opin. Neurobiol.* 6, 475–480.
- Reynaud, A., Barthelemy, F., Masson, G., Chavane, F., 2007. Input–output transformation in the visuo-oculomotor network. *Arch. Ital. Biol.* 145.
- Roland, P.E., 2002. Dynamic depolarization fields in the cerebral cortex. *Trends Neurosci.* 25.
- Salin, P., Bullier, J., 1995. Corticocortical connections in the visual system: structure and function. *Psychol. Bull.* 75, 107–154.
- Saul, A., 2008. Lagged cells. *Neurosignals* 16, 209–225.
- Saul, A., Humphrey, A., 1990. Spatial and temporal response properties of lagged and nonlagged cells in cat lateral geniculate nucleus. *J. Neurophysiol.* 64 (1), 206–224.
- Sharon, D., Grinvald, A., 2002. Dynamics and constancy in cortical spatiotemporal patterns of orientation processing. *Science* 295 (5554), 512–515.

- Sharon, D., Jancke, D., Chavane, F., Na'aman, S., Grinvald, A., 2007. Cortical response field dynamics in cat visual cortex. *Cereb. Cortex* 17 (12), 2866–2877.
- Skottun, B., De Valois, R., Grosof, D., Movshon, J., Albrecht, D., Bonds, A., 1991. Classifying simple and complex cells on the basis of response modulation. *Vis. Res.* 31, 1079–1086.
- Slovin, H., Arieli, A., Hildesheim, R., Grinvald, A., 2002. Long-term voltage-sensitive dye imaging reveals cortical dynamics in behaving monkeys. *J. Neurophysiol.* 88 (6), 3421–3438.
- Stoelzel, C., Bereshpolova, Y., Gusev, A., Swadlow, H., 2008. The impact of an Igdnd impulse on the awake visual cortex: synaptic dynamics and the sustained/transient distinction. *J. Neurosci.* 28 (19), 5018–5028.
- Thomson, A.M., Bannister, A.P., 2003. Interlaminar connections in the neocortex. *Cereb. Cortex* 13, 5–14.
- Thomson, A., Lamy, C., 2007. Functional maps of neocortical local circuitry. *Front. Neurosci.* 1 (1), 19–42.
- Thomson, A., West, D., Wang, Y., Bannister, A., 2002. Synaptic connections and small circuits involving excitatory and inhibitory neurons in layers 2–5 of adult rat and cat neocortex: triple intracellular recordings and biocytin labelling in vitro. *Cereb. Cortex* 12 (9), 936–953.
- Tsodyks, M., Pawelzik, K., Markram, H., 1998. Neurla networks with dynamic synapses. *Neural Comput.* 10 (4), 821–835.